DESIGN OF A TWO-DEGREE-OF-FREEDOM GRIPPER FOR PARALLEL MANIPULATORS

by

Taylan Atakuru

B.S., Mechanical Engineering, Middle East Technical University, 2014

Submitted to the Institute for Graduate Studies in
Science and Engineering in partial fulfillment of
the requirements for the degree of
Master of Science

Graduate Program in Mechanical Engineering

Boğaziçi University

2017

ACKNOWLEDGEMENTS

It would not be possible to complete my thesis without the help of my advisor, Professor Samur. I sincerely thank him for his valuable guidance and support. I would also like to thank Prof. Halil İ. Başẗurk and Prof. Gökhan Kiper who accepted to be jury members of my master's thesis despite their overwhelming busy schedule.

I would also like to thank my friends in Haptics and Robotics lab, including Gholamreza, Onur, Mohammad, Oğuzhan, Alican, Mehdi and Efe.

I would also like to thank HKTM Engineering family, Tunç Atıl, İlham Çelebi, Tolga Cankurt, Selim Küçük and Ahmet Topbaş. They financially supported my thesis and enabled me to make assembly and test of my design in their factory.

Finally, my special thanks go to my family, my lovely mom Nurhan, my dad Tuncay and my beloved sister Seren for their everlasting support and love.

This project is supported by the Ministry of Science, Industry and Technology, Republic of Turkey, TÜBİTAK/SANTEZ project number 0979.STZ.2015.

ABSTRACT

DESIGN OF A TWO-DEGREE-OF-FREEDOM GRIPPER FOR PARALLEL MANIPULATORS

Parallel manipulators are closed-loop mechanisms presenting superior performance compared to serial manipulators in terms of speed, accuracy, precision, and rigidity. They have become widely popular in the industry in the last two decades. Although parallel manipulators are fast enough for most industrial operations, sometimes they cannot catch up with the speed of objects on the conveyor thereby missing some pieces. Considering randomly arriving objects on a conveyor, this task becomes even more challenging. In this study, a two-degree-of-freedom gripper for parallel manipulators is developed in order to overcome this difficulty. First of all, design details of the gripper are presented. Second, preliminary analyses are performed using a three axis Delta-type manipulator for a typical pick-and-place task. Third, the developed gripper is integrated into the same manipulator and tested for certain performance criteria. The analysis and measurement results show that the manipulator performs a given task with reduced cycle time and energy consumption when integrated with the proposed gripper rather than a conventional one.

ÖZET

PARALEL MANİPÜLATÖRLER İÇİN İKİ SERBESTLİK DERECELİ TUTUCU TASARIMI

Paralel manipulatörler kapalı kinematik yapıya sahip, mükabilleri olan seri manipülatörlere göre hız, hassasiyet ve sertlik açısından üstün performans gösteren mekanizmalar olarak tanımlanır. Endüstride, paralel manipülatör kullanımı son yirmi yılda artmaktadır. Ancak paralel manipülatörler hızlı olmalarına rağmen ürün bandından gelen ürünlerin hepsini yakalamakta zorluk yaşıyorlar ve bazı ürünleri kaçırıyorlar. Ürünlerin de bant üzerinde rastgele geldiğini düşünecek olursak, bu görev manipülatörler için daha da zor bir hale gelebiliyor. Bu çalışmada, bahsedilen zorluğun üstesinden gelebilmek için paralel manipülatörlere iki serbestlik dereceli tutucu tasarlandı. Öncelikle, üç eksenli Delta robot kullanılarak bir ön çalışma yapıldı. Daha sonra yine aynı üç eksenli bir manipülatör üzerinde performans testleri yapıldı. Analiz ve test sonuçları gösteriyor ki iki serbestlik dereceli tutucu bir paralel manipülatöre entegre edildiğinde, verilen görev daha kısa sürede ve daha az enerji harcanarak gerçekleştirilebilmektedir.

TABLE OF CONTENTS

LIST OF FIGURES

LIST OF TABLES

LIST OF SYMBOLS

a	Length of the lower arm of the manipulator
a_2	Link length of the crank
a_3	Link length of the connecting rod
a_{G3}	Acceleration of the connecting rod
a_{G3x}	x component of acceleration of the connecting rod
a_{G3y}	y component of acceleration of the connecting rod
b	Length of the lower arm of the manipulator
c	Eccentricity
c_{xi}	x position of point C_i relative to the (x_i, y_i, z_i)
c_{yi}	y position of point C_i relative to the (x_i, y_i, z_i)
c_{zi}	z position of point C_i relative to the (x_i, y_i, z_i)
c_3	Center of mass position of the connecting rod
d	Distance between two objects
d_{center}	Center distance between the pulleys
d_0	Diameter of an object
d_1	Pitch diameter of the small pulley
d_2	Pitch diameter of the large pulley
g_c	Center of gravity
I_m	Axial moment of inertia of the rotor
I_p	Moment of inertia of the large pulley
I_3	Moment of inertia of the connecting rod
K	Total kinetic energy
K_{ai}	Kinetic energy of the input link and the rotor on limb i
K_{bi}	Kinetic energy of the two connecting rods of limb i
K_p	Kinetic energy of the moving platform
L	Lagrangian function
L_{belt}	Length of the belt
m_a	Mass of the input link

m_b	Mass of each connecting rod
m_p	Mass of the platform
m_3	Mass of the connecting rod
m_4	Mass of the slider
p	Center position of the moving platform
P	Position vector of point P
P_i	Power of the i^{th} actuator
p_x	x-component of the point p
p_y	y-component of the point p
p_z	z-component of the point p
$P(x, y)$	Center point of the two-object system
R	Speed ratio of the pulleys
r_s	Stroke of the slider-crank mechanism
s_{14}	Stroke of a slider-crank mechanism
$\dot{s}_{14}$	Velocity of stroke
$\ddot{s}_{14}$	Acceleration of stroke
t_b	Blend time
t_{cycle}	Cycle time
T_d	Torque applied to the small pulley
t_f	Operation time
t_s	Switching time
t_{sub}	Sub path time
T_i	Torque applied by the i^{th} actuator
T_p	Torque applied to the large pulley
T_{12}	Torque applied to the crank
U	Total potential energy
U_{ai}	Potential energy of the input link and the rotor on limb i
U_{bi}	Potential energy of the two connecting rods of limb i
U_p	Potential energy of the moving platform
V_b	Speed of the belt
v_p	Linear velocity of the end effector

v_{G3}	Velocity of the connecting rod
v_{G3x}	x-component of the velocity of the connecting rod
v_{G3y}	y-component of the velocity of the connecting rod
δs_{14}	Uncertainty of the stroke
$\delta\theta_{12}$	Uncertainty of angle of the crank
λ	Lagrangian multiplier
μ	Transmission angle
ω_{ij}	Angular velocity of the j^{th} link of the i^{th} limb
ω_1	Angular velocity of the small pulley
ω_{12}	Angular velocity of the crank
ω_2	Angular velocity of the large pulley
θ	Orientation of the two object
$\ddot{\theta}$	Acceleration of the trajectory
θ_c	Angle of the crank with respect to the horizontal axis
θ_{ij}	Joint angle of the j^{th} link of the i^{th} limb
$\ddot{\theta}_{max}$	Maximum acceleration of the trajectory
θ_{m1}	Required angle to be commanded to the motor on the left
θ_{m2}	Required angle to be commanded to the motors on the right
θ_s	Angle between slider axis and the horizontal axis
θ_1	Angle of contact of the small pulley
θ_2	Angle of contact of the large pulley
θ_{12}	Angle of the crank
θ_{13}	Angle of the connecting rod

LIST OF ACRONYMS/ABBREVIATIONS

DOF	Degrees of Freedom
PM	Parallel Manipulator
PnP	Pick and Place
SM	Serial Manipulator

1. INTRODUCTION

Industrial robots provide numerous advantages to industry. They increase throughput by working faster and more accurately and ultimately boost overall profits. Moreover, they do not need a break and are able to work 24 hours a day [1] thereby decreasing production costs. Furthermore, they help to improve product quality and reliability, reduce waste, and increase safety. Therefore, the demand for industrial robots is dramatically increasing day by day [2]. For instance, parallel manipulators (PMs) have become widely popular in the last two decades [3–5].

PMs can be defined as closed-loop kinematic chains whose end-effectors are linked to the base by at least two independent kinematic chains [6]. As it can be seen in Figure 1.1, PMs are composed of four main parts: actuators, links, joints, and end-effectors. They offer several benefits over serial manipulators (SMs). These advantages include higher load capacity, improved position accuracy, higher stiffness, less vibration, increased acceleration, and most importantly higher speed [7–10]. However, the main drawback of PMs is that they have singularity problems in their limited workspace [11]. PMs and SMs are compared in terms of basic robot features in Table 1.1.

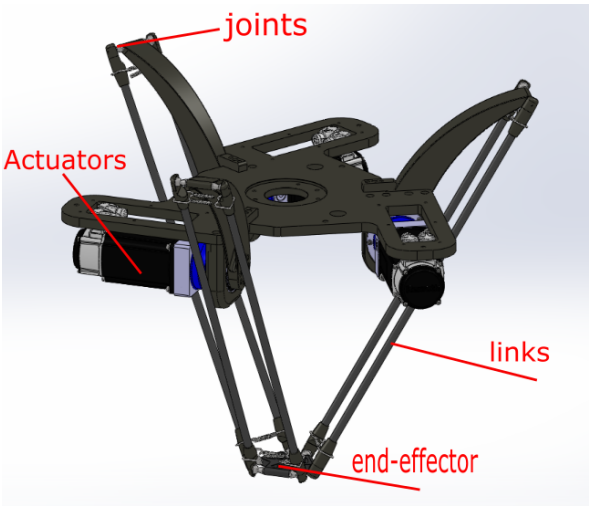

Figure 1.1. A Delta-type parallel manipulator.

Table 1.1. Parallel manipulators vs serial manipulators.

Property	**Parallel Manipulator**	**Serial Manipulator**
Kinematic Chain	Closed loop	Open loop
End-Effector	Platform	Gripper
Location of the Actuators	On the fixed base	On the links
Inertia	Less	High
Stiffness	High	Less
Direct Kinematics	Complicated	Straightforward
Inverse Kinematics	Straightforward	Complicated
Design Considerations	Workspace and Singularities	Stiffness and Vibration

1.1. Aim of the Study

PMs are very fast. For instance, ABB's IRB 360 FlexPicker, which is the most sold parallel manipulator [12], can reach up to 100 pieces per minutes. However, it is observed that even parallel manipulators remain incapable of performing certain tasks, especially in the packaging industry. Although they are very fast, sometimes they cannot catch up with the speed of the objects on the conveyor thereby missing some pieces.

The industry is trying to solve this problem by either using a couple of manipulators (see Figure 1.2) in order to pick up all goods on a production line [13], or reducing the conveyor speed of the line so that no goods are missed. However, these solutions lead to an increase in cost or time of the operation. Alternatively, grippers handling multiple objects (see Figure 1.3), are used as well [14]. This type of gripper is quite useful in industry, especially when the objects arrive in an orderly manner. However, this solution is not that much effective in reducing the cycle time if the objects arrive randomly.

Picking up randomly-arriving multiple objects poses a challenge to the robotic industry. This research is aimed at resolving this problem by designing a new type of gripper. In this study, a novel two degree-of-freedom (DOF) gripper for industrial robots is proposed. The main idea behind this design is to pick two randomly-arriving objects at the same time. Therefore, the novel design, when integrated with an industrial robot, will result in reduced cycle time and reduced energy consumption for a given task.

Figure 1.2. Two IRB 360 FlexPicker robots from ABB picking up objects from a conveyor. Reprinted from [15].

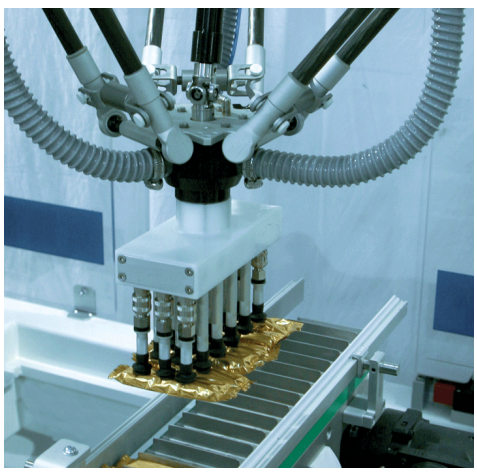

Figure 1.3. A gripper picking up several products. Reprinted from [16].

2. LITERATURE REVIEW

The tasks carried out by a human hand are replaced with more efficient handling equipment, called a gripper [14]. It is arduous for a robotic gripper to compete with a human hand in terms of dexterity [1]. For instance, a six-DOF motion can easily be achieved with a human hand, but not with an advanced and complicated robotic gripper (see Figure 2.1). However, it is inevitable to use grippers in industrial operations when dirty, hazardous, and repetitive works are considered.

Grippers play a crucial role in task performance of robots [17] because they are the parts interacting with the environment. They are capable of completing different tasks depending on the application.

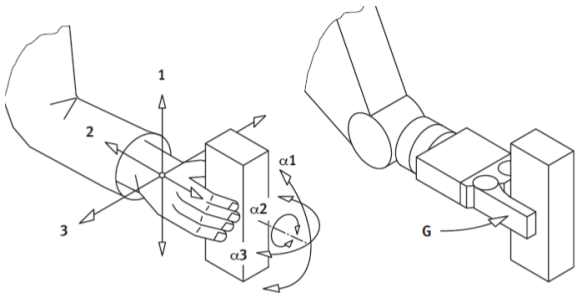

Figure 2.1. 6-DOF motion with; a human hand (left) and a robotic gripper (right). Reprinted from [18].

2.1. Types of Grippers

In this section, grippers are categorized into three main groups according to their structure, number of carried objects, and degree-of-freedom.

2.1.1. Structure

Grippers are classified by three main groups according to their structure: mechanical finger type, vacuum and magnetic type, and universal grippers [19].

Mechanical finger grippers are used to grasp objects by fingers. A photo of a three-finger gripper and a corresponding human hand pose is shown in Figure 2.2. Mechanical fingers hold workpieces by either enclosing them or by clamping with friction force [20]. Besides, motion of fingers is achieved by different mechanisms. They include linkage, rack-and-gear, cam-actuated, screw-driven, pulley-and-rope, and miscellaneous types of mechanisms [19].

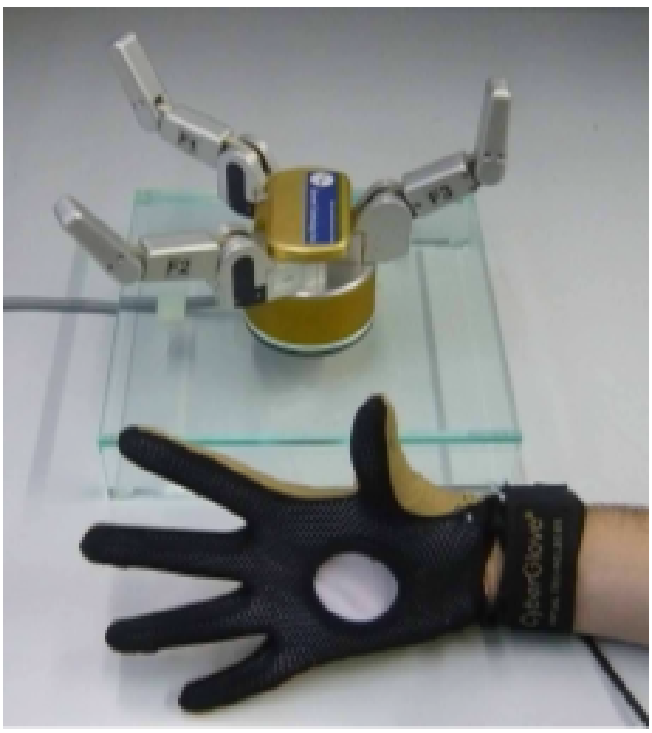

Figure 2.2. A finger type gripper. Reprinted from [21].

As a second group, vacuum grippers hold objects having flat, smooth, and clean surfaces. Components of a typical vacuum gripper are illustrated in Figure 2.3. They are based on suction cups handling the objects by applying pressure difference. When the interior pressure of a suction cup is lower than the atmospheric pressure, suction is achieved. Significant number of handling operations, such as clamping, sorting, feeding, stacking and turning can be performed with suction cups [18]. Therefore, they are widely used in various fields of robotics [22–24], especially in the packaging industry [25].

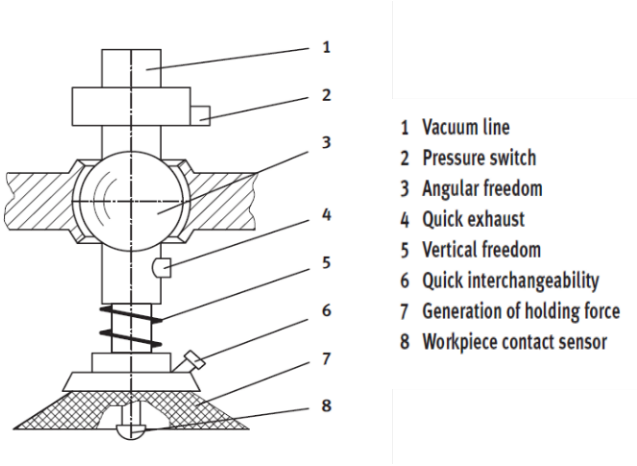

Figure 2.3. Typical components of a vacuum gripper. Reprinted from [18].

Magnetic grippers, on the other hand, are used for holding metal objects. A magnetic gripper in use is shown in Figure 2.4. Although grippers of this type are very fast, they are heavy, and residual electromagnetic problems can be posed [20].

Figure 2.4. A magnetic gripper. Reprinted from [26].

Finally, universal type grippers consist of an elastic membrane filled with mass of granular materials [27]. Granular materials encased in an elastic membrane can conform to the shape of the object to be picked up. Therefore, universal type grippers can pick up a wide variety of arbitrarily shaped objects with different materials, different textures, and different fragility (see Figure 2.5).

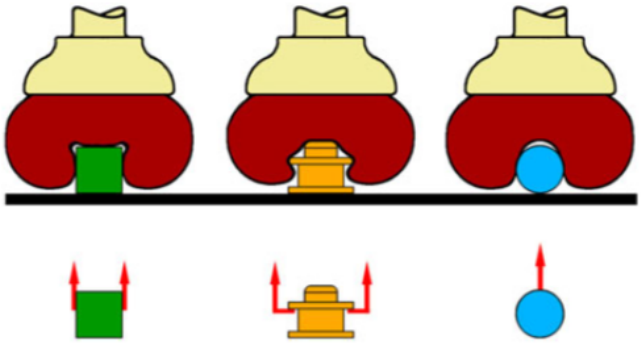

Figure 2.5. Picking up three different shape objects with a universal gripper. Reprinted from [27].

As a summary of this subsection, six different ways to pick up an object is illustrated in Figure 2.6. The first three grippers are of the finger type. The object is enclosed in (1), partially enclosed with clamping force in (2), and clamped in (3). Vacuum and magnetic grippers are shown in (4) and (5), respectively. The last gripper in (6) is of the universal type, using a granular material to pick up the object.

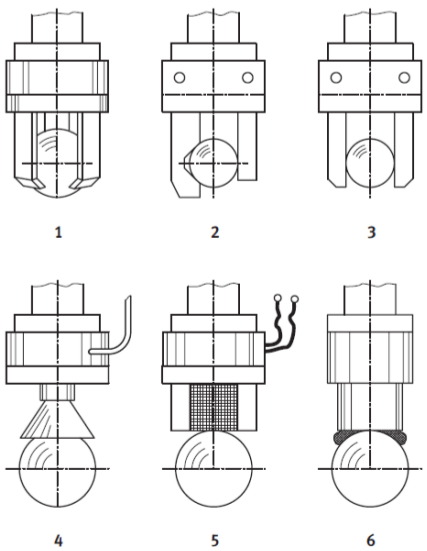

Figure 2.6. An object held with six different grippers. Reprinted from [18].

2.1.2. Number of Carried Objects

Grippers can also be classified according to the number of carried objects. A single gripper can pick up only one object. For example, the grippers shown in Figure 2.6 are single grippers. Double and dual grippers have two grasping devices to pick up two objects. The only difference between them is that dual grippers hold two objects simultaneously (see Figure 2.7) whereas double grippers hold the objects independently (see Figure 2.8). Multiple grippers, on the other hand, hold more than two objects. For instance, gripper shown in Figure 1.3 is a multiple gripper because it holds 6 objects at the same time. Another example of multiple gripper is shown in Figure 2.9. The gripper can pick up four objects, thanks to a rotating lever adjusting the distance between the individual grippers for objects having a defined amount of separation on the conveyor.

Figure 2.7. A dual gripper. Reprinted from [28].

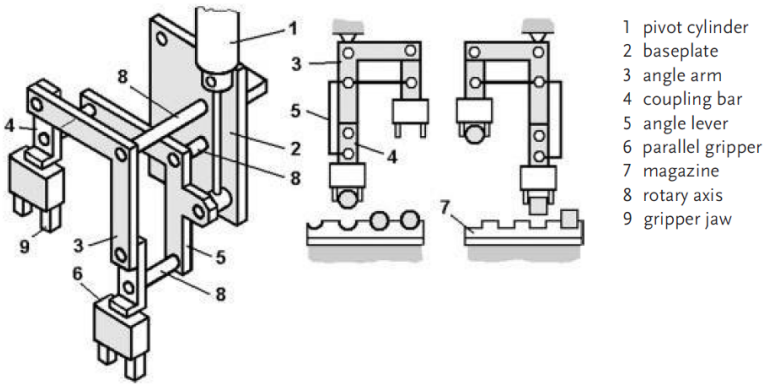

Figure 2.8. A double gripper. Reprinted from [14].

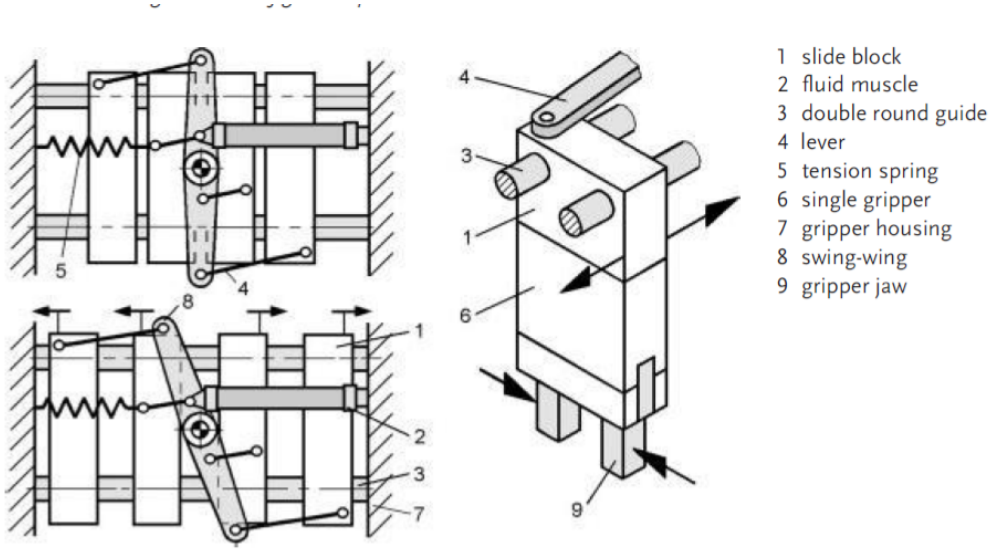

Figure 2.9. A multiple gripper. Reprinted from [14].

2.1.3. Degrees of Freedom

According to DOF, mechanisms of grippers can be divided into three groups. These are immobile, 1-DOF, and multi-DOF grippers. Immobile grippers do not have any DOF. In other words, they have neither a translational nor a rotational DOF. An example of immobile gripper is shown in Figure 1.3. It is an immobile gripper even though multiple objects are held with this gripper. As the second group, 1-DOF grippers have either a translational, a rotational, or combination of rotational and translational DOF. For instance, an example of a 1-DOF gripper having translational DOF is shown in Figure 2.9. On the other hand, Figure 2.10 shows a 1-DOF gripper with a rotational DOF. Please keep in mind that multiplicity of jaws are not taken into account. For instance, the gripper in Figure 2.10 has three more jaws so the mechanism itself has three more DOF. Finally, multi-DOF grippers have more than one DOF. An example of multi-DOF grippers having one translational and one rotational DOF is shown in Figure 2.11. This gripper can position a vacuum suction cup within an adjustment range. Rotational motion is achieved by a stepper motor via a toothed belt gear, and a rack-and-pinion mechanism is used to achieve translational motion.

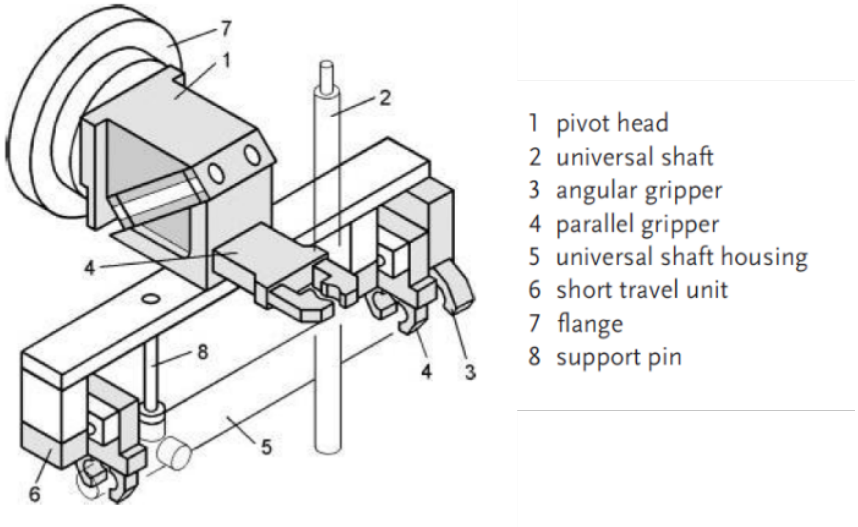

Figure 2.10. 1-DOF gripper having one rotational DOF. Reprinted from [14].

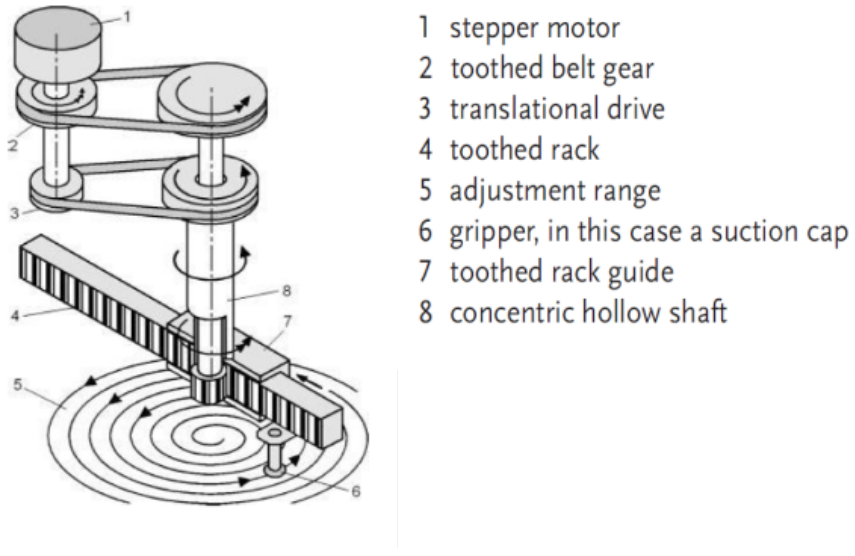

Figure 2.11. Multi-DOF gripper having one rotational and one translational DOF. Reprinted from [14].

To sum up, the grippers are categorized according to their structures, number of carried objects, and degrees of freedom. The proposed gripper in this study falls into the 2-DOF dual vacuum gripper category. Our gripper is capable of picking randomly-arriving two objects simultaneously. It has both translational and rotational DOFs. What makes our design different from the state-of-the-art grippers are shown in Table 2.1.

Table 2.1. The proposed 2-DOF gripper in comparison with the state-of-the-art grippers.

Gripper	**Translational DOF**	**Rotational DOF**	**Picking two object simulataneously**	**Randomly arriving objects**
Figure 2.7	×	✓	✓	×
Figure 2.8	×	✓	×	×
Figure 2.9	✓	×	✓	×
Figure 2.10	×	✓	✓	×
Figure 2.11	✓	✓	×	✓
Our design	✓	✓	✓	✓

3. METHODS AND MATERIALS

In this chapter, design of the 2-DOF gripper is described at first. Second, the design is integrated into a 3-axis Delta Robot. Finally, performance analyses and measurements of the 2-DOF gripper are performed in terms of performance criteria, cycle time and energy reduction.

3.1. 2-DOF Gripper

In this section, design development, analysis, and evaluation methods of the 2-DOF gripper are described. First of all, design requirements are determined that shapes the geometry of the 2-DOF gripper. Second, mechanisms used in the 2-DOF gripper are determined. Third, kinematic analyses and syntheses of the mechanisms are done. Fourth, solid model of mechanical components and the assembly of the 2-DOF gripper are shown. Fifth, working principle of the 2-DOF gripper is analyzed in terms of kinematic parameters. Finally, it is given detailed information about the components and the assembly.

3.1.1. Design Requirements

In this section, design requirements for a dual gripper capable of picking up randomly-arriving two objects are discussed. In order to fully define two point-mass objects on a plane (see Figure 3.1), four parameters are needed. These parameters can be Cartesian coordinates of the two objects; x_1, y_1, x_2, and y_2. Assuming that these coordinates are known, which can be determined through image processing [29], an imaginary line connecting the objects can be drawn. Then, the coordinates of the mid point of this line $[P(x, y)]$, the distance between the objects (d), and the angle between the line and the horizontal axis (θ) can be determined. Since an end effector attached with a gripper can be moved to $P(x, y)$, the number of design parameters for the gripper decreases to two. Therefore, d and θ are selected as two design parameters for a 2-DOF gripper in this study. In other words, a gripper having a translational and a rotational

DOF is required in order to pick up two object simultaneously. Furthermore, it is considered that translational and rotational motions that satisfy the design parameters should be performed rapidly. In other words, these motions should be completed before the manipulator does its work. Therefore, no delay can happen. The target values for θ and d are shown in Table 3.1. Note that d_0 represents diameter of an object to be picked and assumed to be 20 mm for minimum distance of the two objects.

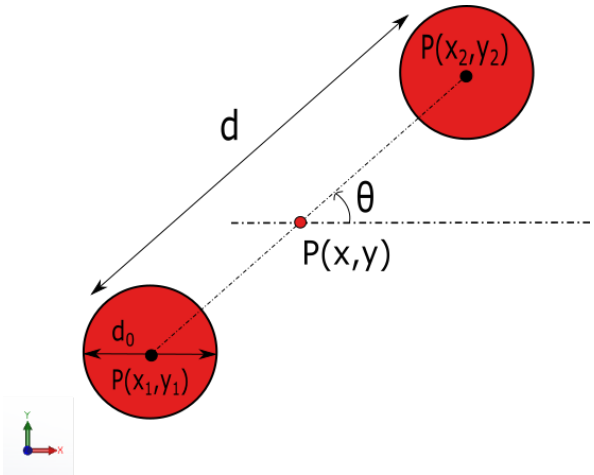

Figure 3.1. Two objects on a planar surface.

Table 3.1. Required minimum and maximum values for the design parameters.

Design Parameters	**min**	**max**
$d \quad (mm)$	20	140
$\theta \quad (deg)$	-90	+90

3.1.2. Functional Synthesis

A 2-DOF gripper including a slider-crank mechanism and a timing belt-pulley mechanism was synthesized in order to satisfy the design requirements, d, and θ respectively. Slider-crank mechanism is a simple mechanism that translates rotational motion to linear motion. Therefore, it is quite popular and used in many applications [30]. The mechanism shown in Figure 3.2 is a centric slider-crank mechanism

with two symmetric sliders. The distance between the two objects (d) is achieved by rotating the crank AA' about point O. On the other hand, a timing-belt-and-pulley mechanism is used to transmit power and motion from a drive shaft to a driven shaft [31]. The principle of this simple transmission is shown in Figure 3.3. Therefore, the orientation θ is achieved by rotating the drive shaft.

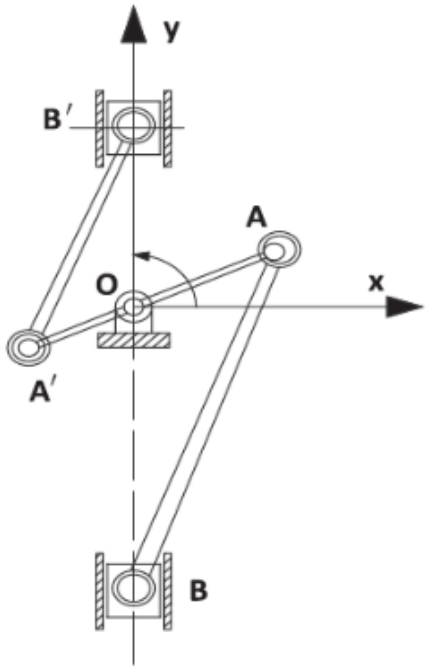

Figure 3.2. A double slider-crank mechanism. Reprinted from [30].

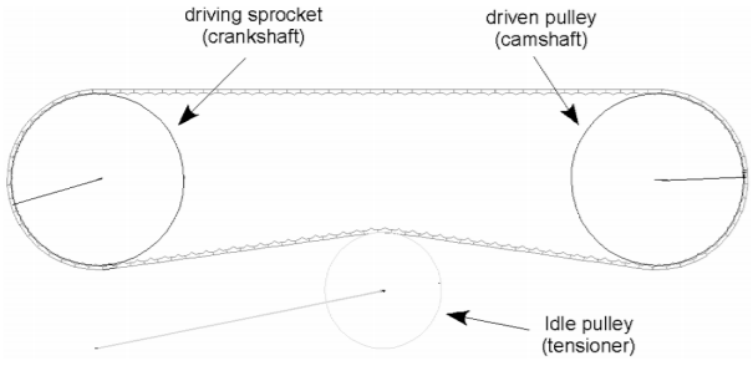

Figure 3.3. A timing belt-pulley mechanism. Reprinted from [32].

3.1.3. Kinematic Analysis

3.1.3.1. Slider-crank kinematic analysis. For a mechanism, desired motion is produced by moving different components of the mechanism relative to each other following certain constraints. The kinematic equations of the slider-crank mechanism are retrieved from [33] written by Eres Söylemez. The geometric parameters of the slider-crank are shown in Figure 3.4. where a_2 is the link length of the crank, a_3 is the link length of the connecting rod, c is the eccentricity, s_{14} is the stroke, θ_{12} is the angle of the crank, θ_{13} is the angle of the connecting rod, and μ is the transmission angle. Assume that the eccentricity, c is zero. Then, the loop closure equation of the slider-crank is

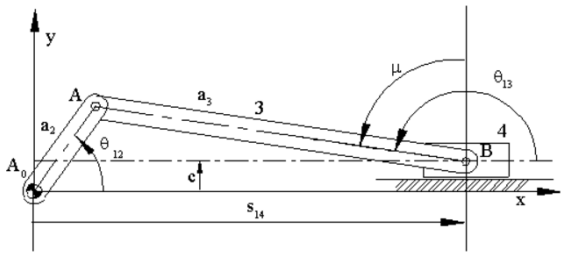

Figure 3.4. Kinematic parameters of a slider crank mechanism. Reprinted from [33].

$$\vec{A_0A} = \vec{A_0B} + \vec{BA} \tag{3.1}$$

The equation can be written with complex numbers in Euler as follows

$$a_2 e^{i\theta_{12}} = s_{14} + a_3 e^{i\theta_{13}} \tag{3.2}$$

Equating x and y component of Equation 3.2, it is obtained as

$$a_2 cos\theta_{12} = s_{14} + a_3 cos\theta_{13} \tag{3.3}$$

$$a_2 sin\theta_{12} = a_3 sin\theta_{13} \tag{3.4}$$

Rewriting Equation 3.3 and Equation 3.4:

$$\theta_{13} = \pi - sin^{-1}(\frac{a_2}{a_3} sin\theta_{12}) \quad for \quad \theta_{13} \geq 90^\circ \tag{3.5}$$

$$s_{14} = a_2 cos\theta_{12} - a_3 cos\theta_{13} \tag{3.6}$$

Taking the derivative of Equation 3.2, it is obtained that

$$ia_2\omega_{12}e^{i\theta_{12}} = \dot{s}_{14} + ia_3\dot{\theta}_{13}e^{i\theta_{13}} \tag{3.7}$$

Complex conjugate of Equation 3.7 is

$$-ia_2\omega_{12}e^{-i\theta_{12}} = \dot{s}_{14} - ia_3\dot{\theta}_{13}e^{-i\theta_{13}} \tag{3.8}$$

Solving for $\dot{s}_{14}$ and $\dot{\theta}_{13}$ by using Equation 3.7 and Equation 3.8, it is obtained as

$$\dot{s}_{14} = a_2 \frac{sin(\theta_{13} - \theta_{12})}{\cos\theta_{13}} \omega_{12} \tag{3.9}$$

$$\dot{\theta}_{13} = \frac{a_2}{a_3} \frac{cos\theta_{12}}{cos\theta_{13}} \omega_{12} \tag{3.10}$$

Taking the derivative of Equation 3.9 and Equation 3.10, assuming that angular velocity, ω_{12}, is constant (for ease of calculation), we obtain the acceleration terms:

$$\ddot{s}_{14} = a_2 \frac{cos\theta_{12}\dot{\theta}_{13} - cos\theta_{13}cos(\theta_{13} - \theta_{12})\omega_{12}}{cos^2\theta_{13}}\omega_{12} \tag{3.11}$$

$$\ddot{\theta}_{13} = \frac{a_2}{a_3} \frac{cos\theta_{12}sin\theta_{13}\dot{\theta}_{13} - cos\theta_{13}sin\theta_{12}\omega_{12}}{cos^2\theta_{13}}\omega_{12} \tag{3.12}$$

In order to find velocity and acceleration of the connecting rod, let the center of mass of the connecting rod be at point G_3 such that

$$AG_3 = c_3$$

Location of G_3 can be found as

$$\vec{A_0G_3} = \vec{A_0B} + \vec{BG_3} = s_{14} + (a_3 - c_3)e^{i\theta_{13}} \tag{3.13}$$

Taking derivative of Equation 3.13, we obtain

$$\vec{v}_{G3} = \dot{s}_{14} + i(a_3 - c_3)e^{i\theta_{13}}\dot{\theta}_{13} \tag{3.14}$$

x and y components of Equation 3.14 are

$$v_{G3x} = \dot{s}_{14} - (a_3 - c_3)sin\theta_{13}\dot{\theta}_{13} \tag{3.15}$$

$$v_{G3y} = (a_3 - c_3)cos\theta_{13}\dot{\theta}_{13} \tag{3.16}$$

Taking derivative of Equation 3.14, we obtain

$$\vec{a}_{G3} = \ddot{s}_{14} + i(a_3 - c_3)e^{i\theta_{13}}\ddot{\theta}_{13} - (a_3 - c_3)e^{i\theta_{13}}\dot{\theta}_{13}^2 \tag{3.17}$$

x and y components of Equation 3.17 are

$$a_{G3x} = \ddot{s}_{14} - (a_3 - c_3)sin\theta_{13}\ddot{\theta}_{13} - (a_3 - c_3)cos\theta_{13}\dot{\theta}_{13}^2 \tag{3.18}$$

$$a_{G3y} = (a_3 - c_3)cos\theta_{13}\ddot{\theta}_{13} - (a_3 - c_3)sin\theta_{13}\dot{\theta}_{13}^2 \tag{3.19}$$

Virtual work method [34] is used for dynamic analysis of the slider-crank mechanism. Virtual work principle states that

$$\delta U_T = \sum_j \vec{F}_j \cdot \delta\vec{r}_j + \sum_j \vec{T}_j \cdot \delta\vec{\theta}_j = 0 \tag{3.20}$$

where F_j and T_j terms includes both external and inertial forces and torques. Therefore, Equation 3.20 can be extended as:

$$\delta U_T = \sum_j \vec{F}_j^e \cdot \delta\vec{r}_j + \sum_j \vec{T}_j^e \cdot \delta\vec{\theta}_j + \sum_j -m_j\vec{a}_{Gj} \cdot \delta\vec{r}_{Gj} + \sum_j -I_j\vec{\alpha}_j \cdot \delta\vec{\theta}_j = 0 \tag{3.21}$$

Assuming there are no external forces,torque value of the slider-crank mechanism can be found by using Equation 3.21

$$T_{12} = \frac{1}{\omega_{12}}\left[(m_4\ddot{s}_{14})\dot{s}_{14} + m_3(a_{G3x}v_{G3x} + a_{G3y}v_{G3y}) + (I_3\ddot{\theta}_{13})\dot{\theta}_{13}\right] \tag{3.22}$$

where I_3 is the moment of inertia of the connecting rod, and m_3 and m_4 are the masses of the connecting rod and slider respectively.

3.1.3.2. Timing belt-pulley kinematic analysis. Geometry of the timing belt pulley mechanism is shown in Figure 3.5. Where d_1 and d_2 are the pitch diameters, and θ_1 and θ_2 are the angle of contact of the driving (small) and the driven (large) pulleys respectively. Moreover, d_{center} is the center distance between the pulleys, and d_{span} is the distance the belt spans between the pulleys. These geometric parameters are expressed in Equations 3.23 to 3.26. Please note that friction effects are ignored.

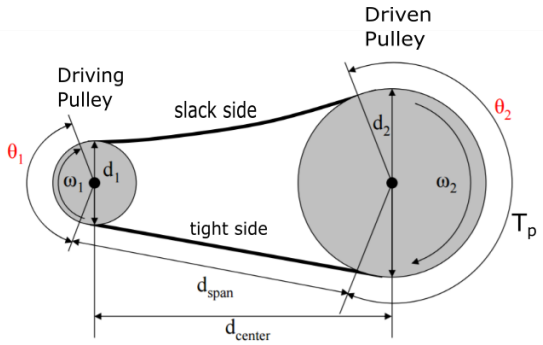

Figure 3.5. Belt drive geometry. Reprinted from [35].

$$\theta_1 = \pi - 2sin^{-1}(\frac{d_2 - d_1}{2d_{center}}) \tag{3.23}$$

$$\theta_2 = \pi + 2sin^{-1}(\frac{d_2 - d_1}{2d_{center}}) \tag{3.24}$$

$$d_{span} = \sqrt{d_{center}^2 - (\frac{d_2 - d_1}{2})^2} \tag{3.25}$$

$$L_{belt} = \sqrt{4d_{center}^2 - (d_2 - d_1)^2} + \frac{1}{2}(d_1\theta_1 + d_2\theta_2) \tag{3.26}$$

Speed of the belt is calculated as

$$V_b = \frac{d_1}{2}\omega_1 = \frac{d_2}{2}\omega_2 \tag{3.27}$$

where ω_1 and ω_2 are the angular speeds of the small and large pulleys, respectively. Moreover, it can be seen from Equation 3.28 that R is defined as the speed ratio of the pulleys.

$$R = \frac{d_1}{d_2} = \frac{\omega_2}{\omega_1} = \frac{T_d}{T_p} \tag{3.28}$$

where T_d is the applied torque to the driven pulley, and T_p is the output torque of the driven pulley. Specifically,

$$T_p = I_p\omega_2 \tag{3.29}$$

where I_p is the moment of inertia of the driven pulley.

3.1.4. Kinematic Synthesis

3.1.4.1. Slider-crank kinematic synthesis. Synthesis of the slider-crank mechanism is composed of mathematically determining geometry of the members to meet the design requirements. An iterative approach was followed for the kinematic synthesis. In this part, dimensions of the links of the slider-crank mechanism were first guessed and then the resultant performance was checked by analysis. Second, the dimensions were modified based on the performance of the previous selections, and adjusted until the desired results were obtained. In other words, the process of iterative synthesis and analysis was repeated to obtain an acceptable design. It is indicated in Table 3.1 that design parameter d, ranges from 20 mm to 140 mm. 140 mm is achieved when the slider-crank is fully stretched out $[d = 2(a_2 + a_3)]$ and 20 mm is achieved when it is in folded back $[d = 2(a_3 - a_2)]$ position. Therefore, link lengths of the crank and the connecting rod of slider crank mechanism can be found as 30 mm and 40

mm respectively. The link lengths of the crank and connecting rod and corresponding masses, and inertia of the connecting rod are shown in Table 3.2.

Table 3.2. Properties of the slider-crank mechanism.

Property	a_2 (m)	a_3 (m)	c_3 (m)	m_3 (kg)	m_4 (kg)	I_3 (kgm^2)
value	0.03	0.04	0.02	0.01	0.4	5.33E-05

Transmission angle ($\mu = \theta_{13} - 90°$) is a significant design parameter for mechanisms [36]. Corresponding transmission angle of the synthesized mechanism is plotted for a full cycle of the crank in Figure 3.6. It can be inferred from this figure that the transmission angle deviates at most 45° from 90°, which is an acceptable value [37]. Assuming an angular speed (ω_{12}) of 100 rpm for the crank, torque requirement for a full cycle was calculated using Equation 3.22. The result is shown in Figure 3.7. Please keep in mind that torque values from Equation 3.22 was multiplied by two because two slider-crank mechanisms are combined in our design as shown in Figure 3.2.

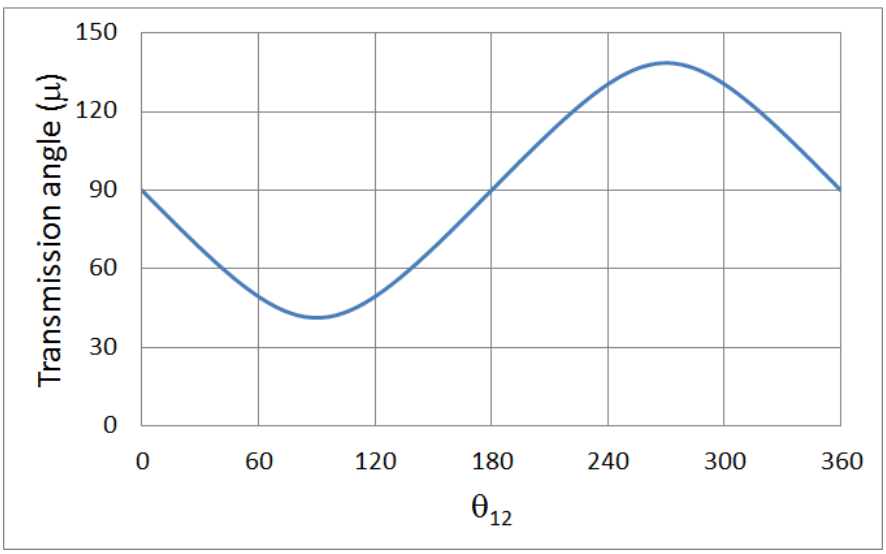

Figure 3.6. Transmission angle of the slider crank mechanism for a full cycle.

It can be seen from Figure 3.7 that maximum torque value is below than 0.1 Nm. Therefore, a suitable motor (Bosch Rexroth MSM019A-300) was selected for continuous operation. Characteristic of the motor is shown in Appendix A.

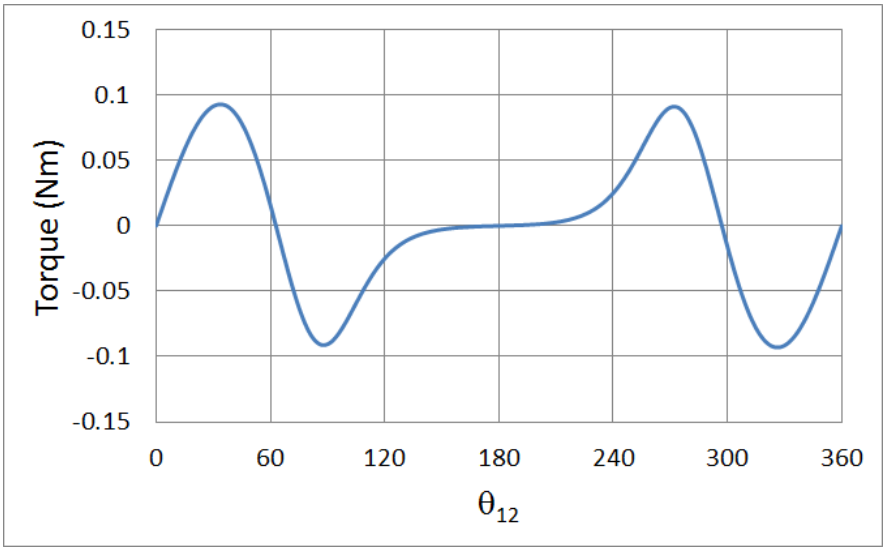

Figure 3.7. Torque required to rotate the crank at 100 rpm with respect to crank angle.

3.1.4.2. Timing belt-pulley kinematic synthesis. Kinematic parameters of the timing belt pulley mechanism are shown in Table 3.3. Number of teeth of the small and the large pulley are selected as 18 and 36 respectively. Therefore, the torque requirement for the small pulley is twice higher than the large pulley (refer to Equation 3.28).

Table 3.3. Features of the timing belt pulley mechanism.

Attribute	**Value**
Speed Ratio	0.50
Pitch Diameter - Large Pulley (mm)	57.3
Pitch Diameter - Small Pulley (mm)	28.6
Belt Pitch Length (mm)	245
Number of Teeth - Belt	49
Center Distance of the Pulleys (mm)	53.1
Teeth in Mesh	7

3.1.5. Mechanical Design

Based on the synthesized mechanisms described in the previous sections, a 2-DOF gripper has been designed. Solid model of the 2-DOF gripper is shown in Figure 3.8. The gripper consists of two actuators (1a) and (1b), a stationary platform (2), a moving platform (3), a timing belt pulley mechanism (A), a slider-crank mechanism (B), and a vacuum suction system (C). Moreover, section view of the 2-DOF gripper can be seen in Figure 3.9. The timing belt-pulley mechanism (A) is composed of a small timing pulley (4) and a large timing pulley (5). The slider-crank mechanism (B) consists of a crank (6), and two connecting rods (7). The vacuum suction system (C) is comprised of two vacuum holders (8), and two connection components (9). The connection components (9) serve as a bridge between the vacuum holders (8) and the connecting rods (7). The motor on the left (1a) actuates the small pulley (4), and movement is transmitted to the large pulley (5) via a timing belt. The large pulley (5) is fastened to the moving platform (3) so that they can move together. An angular contact ball bearing (10) is placed between the large pulley (5) and a connection component (11). The inner race of the bearing fits on the connection component (11) while the outer race of the bearing fits inside the large pulley (5). The motor on the right (1b) actuates the slider-crank mechanism (B). Since the length of the motor shaft is not long enough, a coupling (12) is used. When the slider crank mechanism (B) is actuated, two carriages (13) slides along the rail (14) thanks to two more connection components (15) placed between the carriages (13) and the connecting rods (7). Therefore, rotation motion is translated to linear motion.

3.1.6. Working Principle

Since two objects are to be held simultaneously, positions of the two objects and the vacuum holders of the gripper must be matched (see Figure 3.10). Where θ_c is the angle of the crank with respect to the horizontal axis, θ_s is the angle between slider axis and the horizontal axis, and r_s is the stroke of the slider-crank mechanism. It can be inferred from Figure 3.10 that the parameters; $P(x, y)$, θ, and d must be equal to the kinematic parameters of the gripper; center point (O), θ_s, and r_s respectively.

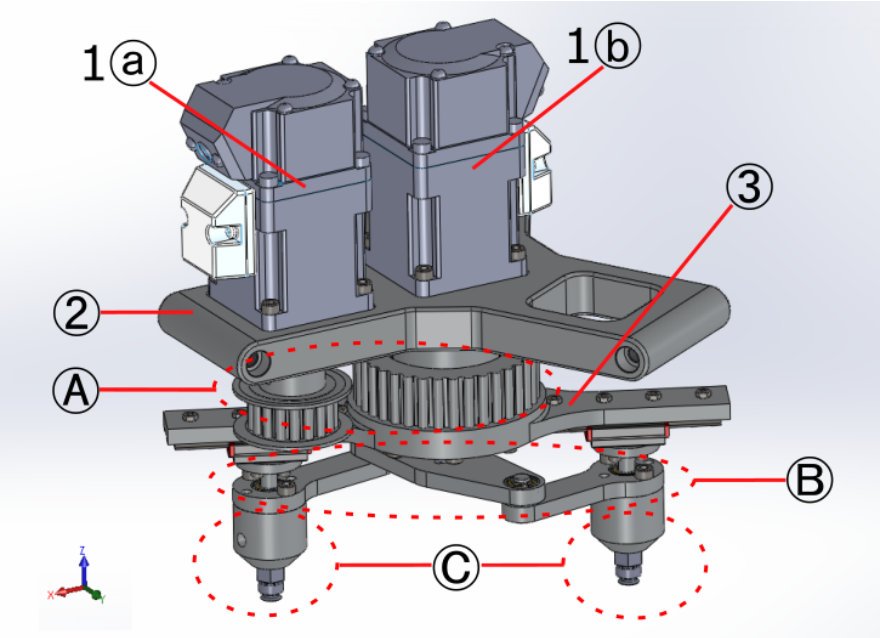

Figure 3.8. 3D model of the 2-DOF gripper.

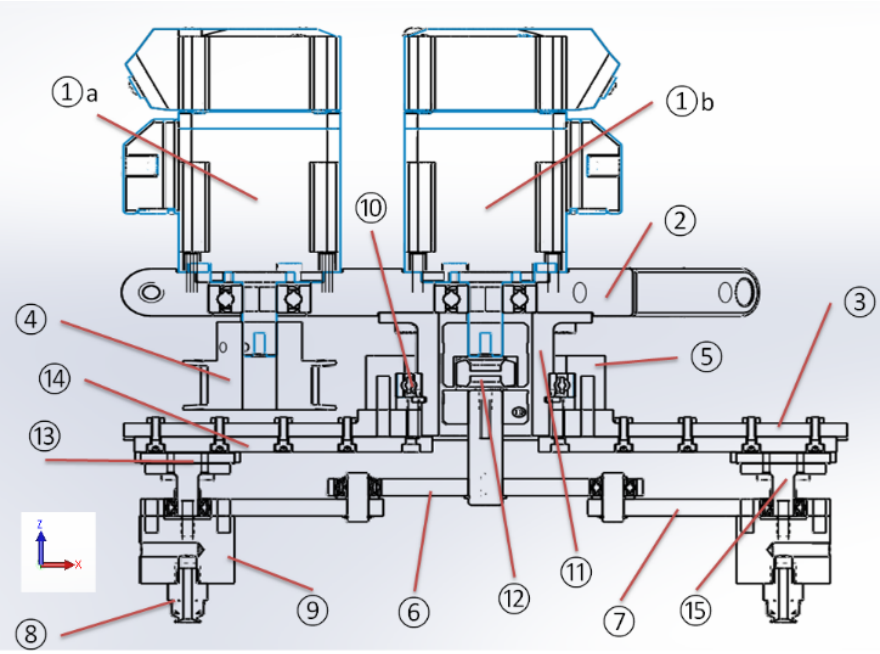

Figure 3.9. Section view of the 2-DOF gripper design.

Therefore, three movements are required to match the kinematic parameters. First, the gripper is moved by means of a manipulator such that the center point (O) coincides with $P(x, y)$. Second, the whole slider-crank mechanism is rotated by the timing-belt pulley mechanism so that the moving platform pivots around its center point, O, until θ_s becomes equal to θ. The final movement is that the motor on the right actuates the slider-crank mechanism, and r_s is matched to the distance between two objects, (d). The overall operation principle is summarized in Figure 3.11. Please note that these three motions can be executed simultaneously.

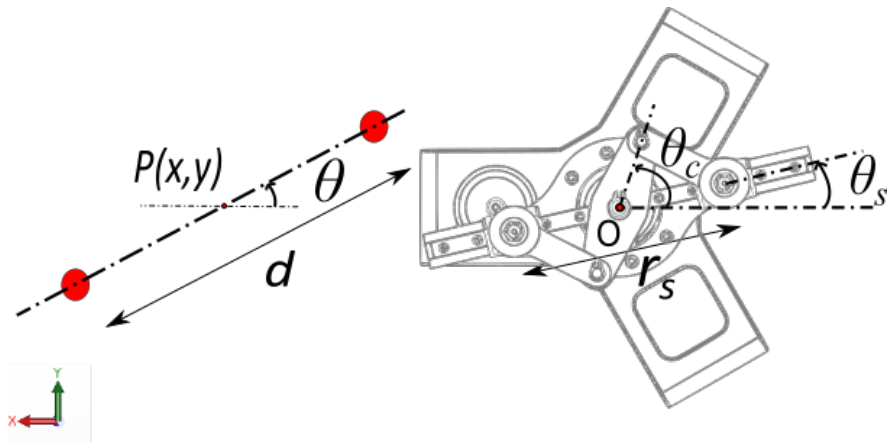

Figure 3.10. Configurations to be matched: Layout of a two-object system on a conveyor (left), and bottom view of the 2-DOF gripper design (right).

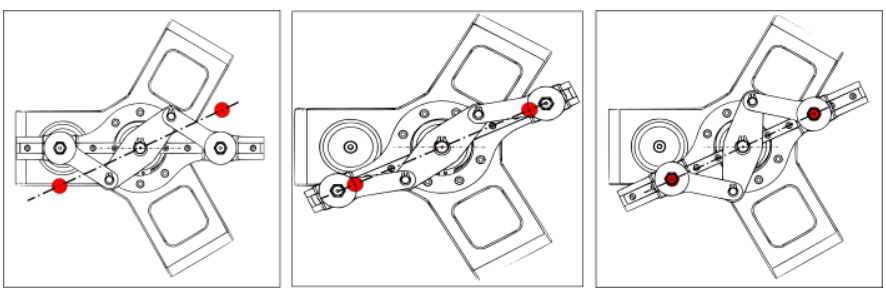

Figure 3.11. Operation principle of the 2-DOF gripper. (Left) The first movement. (Middle) The motor on the left rotates the small pulley to a desired orientation (θ). (Right) The motor on the right rotates the crank so that the distance between the vacuum holders (r_s) is matched to a desired distance (d).

Suppose that there are n pairs of randomly-arriving objects to be picked up. Poses; orientation, (θ^n) and distance, (d^n), of each pair are assumed to be known through image processing. Superscript n represents n^{th} pair of randomly-arriving objects. The required angles to be commanded to the motors are θ^n_{m1} and θ^n_{m2} in order to match θ^n_s, and r^n_s, to the desired pose θ^n and d^n, respectively. Since θ_s=θ, the motor on the left is commanded by amount of, θ^n_{m1}, as follows

$$\theta^n_{m1} = \left[\theta^n - \theta^{n-1}\right] \times \frac{1}{R} \tag{3.30}$$

From the forward kinematics of slider-crank mechanism (refer to Equation 3.6), the stroke, r^n_s is calculated as

$$r^n_s = 2\left[a_2 cos\theta^n_{12} - a_3 cos\left[sin^{-1}(\frac{a_2}{a_3} sin\theta^n_{12})\right]\right] \tag{3.31}$$

Since r^n_s=d^n, θ^n_{12} can be determined from Equation 3.31:

$$\theta^n_{12} = cos^{-1}\left(\frac{a_2^2 - a_3^2 + (\frac{d^n}{2})^2}{a_2 d^n}\right) \tag{3.32}$$

From Figure 3.10, it can be seen that

$$\theta^n_c = \theta^n_{12} + \theta^n_s \tag{3.33}$$

Therefore, the motor on the right is commanded by amount of, θ_{m2}, as follows

$$\theta^n_{m2} = \left[\theta^n_c - \theta^{n-1}_c\right] \tag{3.34}$$

3.1.7. Prototype Development

A prototype of the 2-DOF gripper has been developed. A photo of the prototype is shown in Figure 3.12.In the following sections, details of the prototype are given.

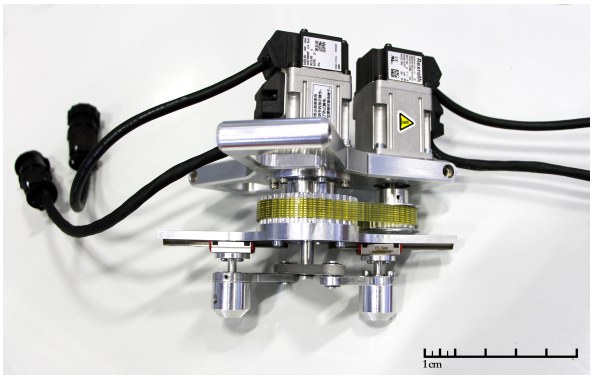

Figure 3.12. 2-DOF gripper prototype.

3.1.7.1. Components. The components of the 2-DOF gripper are divided into two groups: the purchased components and the manufactured components. The purchased are shown in Table 3.4. On the other hand, the manufactured components are shown in Table 3.5. Technical drawings of the manufactured components of the 2-DOF gripper are given in the Appendix B.

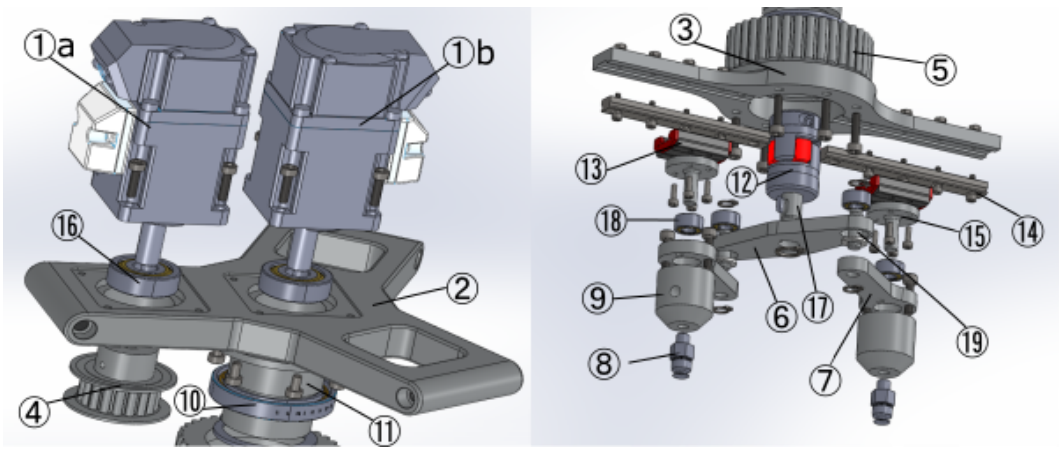

Figure 3.13. Components of the 2-DOF gripper in an exploded view.

Table 3.4. Purchased parts of the 2-DOF gripper.

Part	**Part / Model**	**item**
Actuators	Bosch Rexroth MSM019A-0300	2
Timing belt pulley system	Large Pulley: 18-T5-B10F	1
	Small Pulley: 36-T5-B10F	1
	Timing Belt: T5 245	1
Linear guide system	Carriage: Schneeberger MNN7	2
	Rail: Schneeberger MNN7	1
Bearings	SKF 61806-2RHSH	1
	NSK 685 ZZ	4
	NMB 628 ZZ	2
Coupling	Kulkarni CS 09	1
Vacuum Components	Ejector: Schmalz SCPS 07 G2 NC M12-5 PNP	1
	Suction Cup: Schmalz PFYN 6 SI-55 M5-AG	2

Table 3.5. Manufactured components of the 2-DOF gripper.

Part	**Manufacturing Method**	**Material**	**Quantity**
Stationary Platform	CNC milling + turning	Al 7075	1
Moving Platfrom	CNC milling + turning	Al 7075	1
Large Pulley	CNC milling + turning	Al 7075	1
Connection Component (11)	CNC milling + turning	Al 7075	1
Crank	CNC milling	Al 7075	1
Connecting Rod	CNC milling	Al 7075	2
Connection Component (9)	CNC milling + turning	Al 7075	2
Connection Component (15)	CNC milling + turning	Al 7075	2
Shafts	CNC turning	Al 7075	2

3.1.7.2. Assembly. The components (indicated with bracketed numbers in Figure 3.13) of the 2-DOF gripper were assembled in the following order:

(i) The bearings (16) were fitted to the stationary platform (2).

(ii) The motors (1a) and (1b) were attached to the stationary platform (2).

(iii) One end of the coupling (12) was attached to motor (1b) while the other end was attached to the shaft (17).

(iv) The connection component (11) was mounted on the stationary platform (2).

(v) Outer race of the bearing (10) were fitted on the inner surface of the large pulley (5).

(vi) Inner race of the bearing (10) were fitted on the outer surface the connection component (15).

(vii) The small pulley (4) was attached to the motor (1a) shaft.

(viii) The timing belt was placed to connect the small pulley (4) and the large pulley (5).

(ix) The moving platform (3) was screwed and pinned on the large pulley (5).

(x) The rails (14) were screwed on the moving platform (3).

(xi) The carriages (13) were placed on the rails (14).

(xii) The connection components (15) were screwed on the carriages (13).

(xiii) The crank (6) was fixed to the shaft (17) using key

(xiv) Two of the identical four bearings (18) were fitted to the holes of the crank (6), while the other two were fitted to the holes of the connecting rod (7).

(xv) One end of the connection component (9) was screwed on the connecting rod (7), while the other end was connected to the vacuum suction holder (8). The procedure was repeated two times.

(xvi) One end of the connecting rod (7) was fitted to connection component (15), while the other end is fitted to the crank (6) by using the shaft (19). The procedure was repeated two times.

Some pictures were taken during the assembly process (see Figure 3.14). There were some difficulties that were solved. First of all, it was realized that geometric tolerances of some parts were not manufactured properly. For instance, hole diameters of the crank did not fit the outer diameter of the bearings. It was supposed to be H7/h6 tolerance but the hole tolerance was not in the range of H7. Instead, a set screw was stripped from both sides of the crank in order to secure the bearing. Second, the coupling was touching the inner surface of the connection component when the motor shaft was rotating. It was due to a misalignment of the coupling. The clearance between outer diameter of the coupling and inner diameter of the connection component was only 1 mm. Therefore, the inner diameter of the connection component was enlarged to 2 mm.

Figure 3.14. Assembly of the mechanical parts of the 2-DOF gripper.

3.1.8. Characterization

3.1.8.1. Speed measurements. As mention in the design requirement, the 2-DOF gripper should take the required configuration before the manipulator moves to the target area. In order to scan the whole workspace, the vacuum holders must move between the edges of the workspace as fast as possible, and the moving platform must rotate 90°. Therefore, speeds of the translational motion (from minimum to maximum stroke) and rotational motion (from 0° to 90°) were tested. The slider-crank mechanism was actuated by the motor (1b). It was moved back and forth twice passing through the maximum and minimum strokes. On the other hand, the timing pulley-belt mechanism was actuated by the motor (1a). It was rotated 90° four times.

3.1.8.2. Position resolution. In this section, position sensing of the stroke, r_s, is calculated. Remember that the stroke was obtained in terms of actuated angle, θ_{12} from Equation 3.31

$$r_s = 2\big[a_2 cos\theta_{12} - a_3 sin^{-1}(\frac{a_2}{a_3} sin\theta_{12})\big] \tag{3.35}$$

As it can be seen from the Equation 3.35, r_s depends only θ_{12}. Let δr_s and $\delta\theta_{12}$ be uncertainties of the stroke and the actuated angle respectively. Therefore, the uncertainty of the stroke can be written as

$$\delta r_s = \frac{\partial r_s}{\partial \theta_{12}} \delta\theta_{12} \tag{3.36}$$

Taking partial derivative of Equation 3.35, Equation 3.37 is found as

$$\delta r_s = 2\Bigg[- a_2 sin\theta_{12} - \frac{a_2 cos\theta_{12}}{\sqrt{1 - (\frac{a_2}{a_3} sin\theta_{12})^2}} \Bigg] \delta\theta_{12} \tag{3.37}$$

3.1.8.3. Repeatability measurements. Repeatability test was performed on the stroke of the slider crank mechanism under identical conditions. The measurements were made by an electronic caliper with precision of 10 microns. The test was repeated 10 times. Please note that the target stroke was 50 mm.

3.2. Integration into a Parallel Manipulator

In order to test whether the 2-DOF gripper design satisfies the performance criteria, our gripper has been integrated with a 3-DOF parallel manipulator developed by HKTM A.Ş. (see Figure 3.15). It is a Delta-type manipulator [38] which has only translational DOF. The vacuum components were connected to the two suction holders of the 2-DOF gripper. Please note that the vacuum command were activated when picking the objects and deactivated when placing them to the desired location. The assembled prototype has been integrated with vacuumed suction components and attached to the parallel manipulator as shown in Figure 3.16.

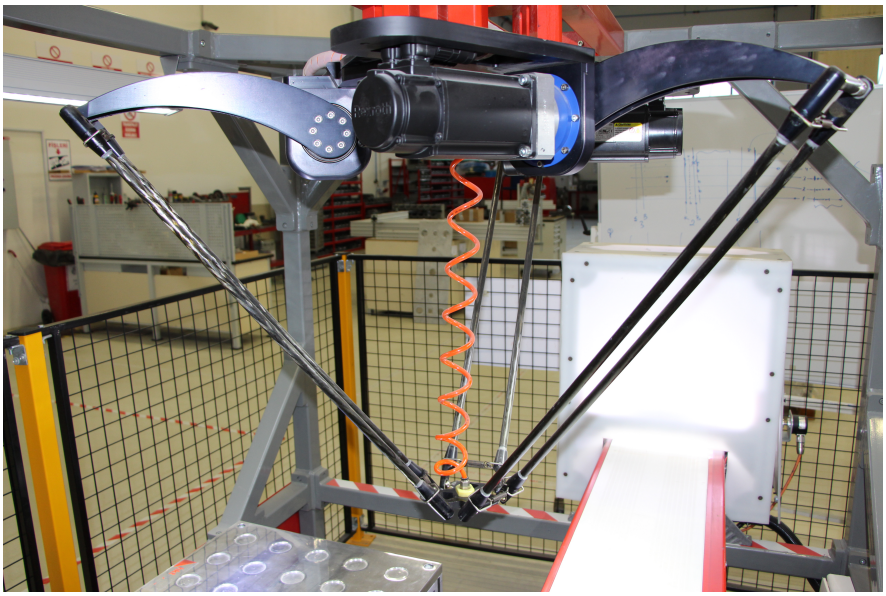

Figure 3.15. A Delta-type parallel manipulator developed by HKTM.

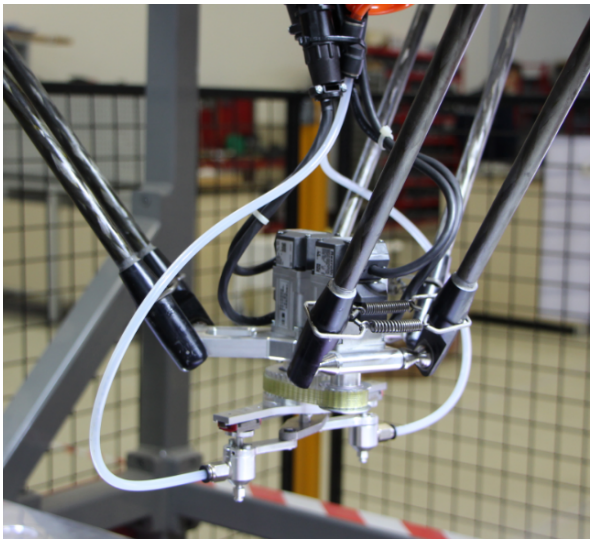

Figure 3.16. 2-DOF gripper prototype attached to the parallel manipulator.

3.2.1. Robot Analyses of a Delta Manipulator

A 3-DOF parallel manipulator developed at the University of Maryland [39] is used for robot analyses. Moreover, dynamic equations of the Maryland manipulator are retrieved from [40] written by Lung-Wen Tsai (Appendix C). It can be seen from Figure 3.17 that this manipulator possesses only translational motion in Cartesian space. Three identical limbs bridge a moving platform to a fixed base. Each limb is composed of an upper and a lower arm; connected by revolute joints. Each upper arm has a parallelogram loop. Besides, revolute joints are used for the parallelogram instead of ball joints employed in the original DELTA robot [38].

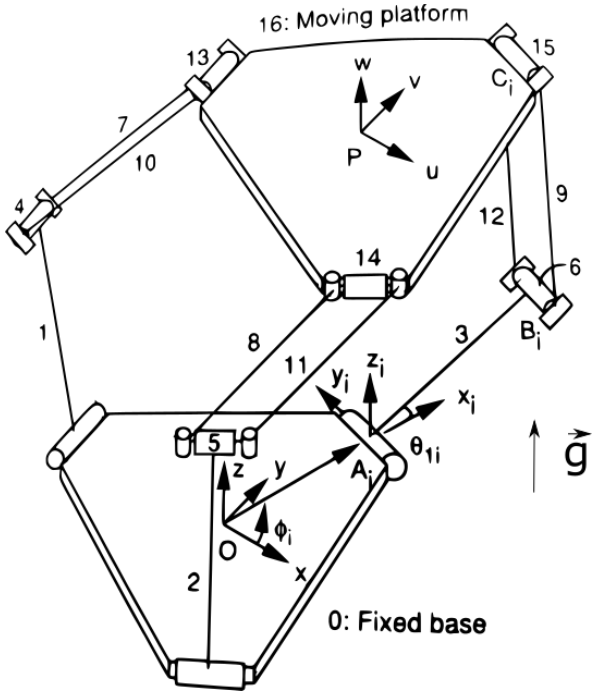

Figure 3.17. Schematic drawing of the Maryland Manipulator. Reprinted from [40].

3.2.2. Trajectory Generation

Motion of a manipulator is usually considered as motion of the tool frame relative to a stationary frame [41]. For this reason, the tool frame moves from its initial value to a final value when the manipulator moves from its current position to the desired position. Please keep in mind that both orientation and position (or simply

configuration) of the tool frame will change continuously relative to the fixed frame. Therefore, the motion must be defined in details by assigning intermediate via points between the initial and final position.

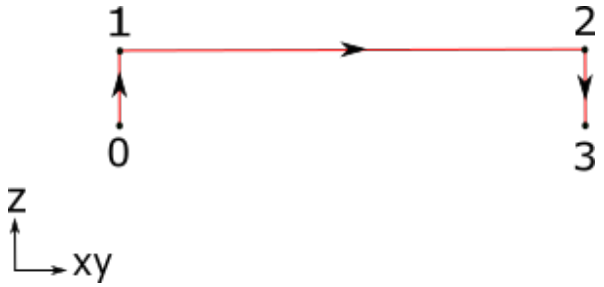

Figure 3.18. Benchmark path to be followed by the manipulator.

A benchmark path was described in Cartesian space for a pick-and-place motion (see Figure 3.18). The manipulator starts at point 0, then moves up along the z-axis and reaches point 1, then moves parallel to the xy plane and reaches point 2, and finally moves down along the z-axis and reaches point 3. Although the path was defined in Cartesian space, a joint-space trajectory was generated for each sub-path (0 to 1, 1 to 2, and 2 to 3). By using inverse kinematics, via points are converted into a set of joint angles, so that a smooth trajectory profile is obtained for each joint that passes through the corresponding via points and the desired points. There are several possibilities for the trajectory, however, the angular velocities of the joints must be continuous especially at the beginning and end of the motion. Therefore, a linear function with parabolic blends [41] was chosen in order to create a smooth trajectory with continuous position and velocity.

As it can be seen in Figure 3.19, velocity is changed smoothly at the blend points, $t = t_b$ and $t = t_f - t_b$, and angular acceleration is changed at those points. Moreover, the path shape is always symmetric about the halfway point in position, θ_h (see Figure 3.20). Therefore, the following equations can be written as

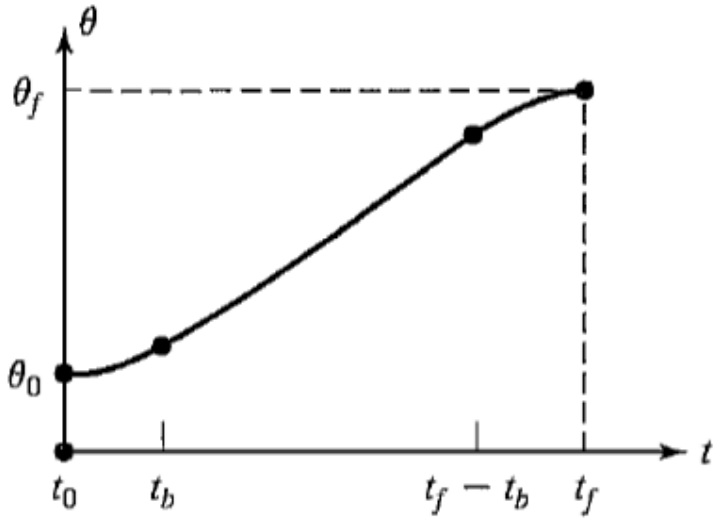

Figure 3.19. Linear segment with parabolic blends. Reprinted from [41].

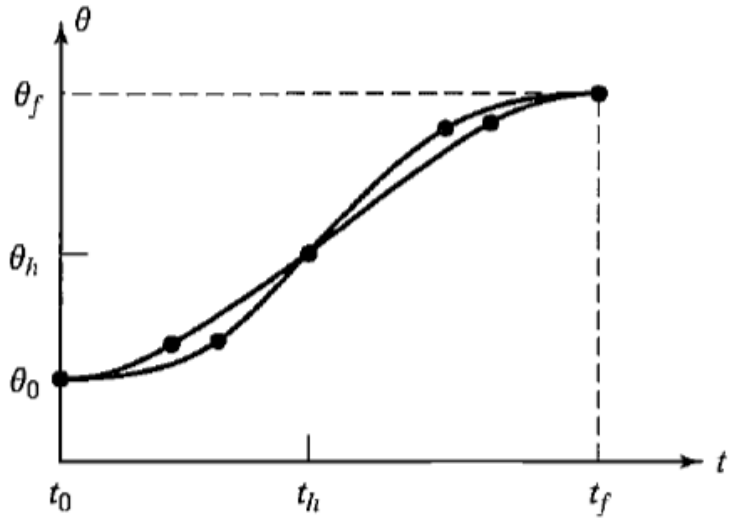

Figure 3.20. Linear segment with parabolic blend at the halfway point. Reprinted from [41].

$$\ddot{\theta} t_b = \frac{\theta_h - \theta_b}{t_h - t_b} \tag{3.38}$$

$$\theta_b = \theta_0 + \frac{1}{2}\ddot{\theta} t_b^2 \tag{3.39}$$

where θ_b is the angle at the end of the blend region, and $\ddot{\theta}$ is the acceleration during the blend region. When the Equation 3.38 and 3.39 are combined, it is obtained

$$\ddot{\theta} t_b^2 - \ddot{\theta} t t_b + (\theta_f - \theta_0) = 0 \tag{3.40}$$

When Equation 3.40 is solved for t_b , it is obtained

$$t_b = \frac{1}{2} - \frac{\sqrt{\ddot{\theta}^2 t^2 - 4\ddot{\theta}(\theta_f - \theta_0)}}{2\ddot{\theta}} \tag{3.41}$$

Normally, an acceleration ($\ddot{\theta}$) is chosen reasonably high in order to have a better solution. However, minimum-time trajectory (see Figure 3.21) is selected due to the fact that it requires maximum acceleration which tests the manipulator at its limits. This is also called as a Bang Bang trajectory [42]. It is because the fastest solution is obtained when maximum acceleration value ($+\ddot{\theta}$) is suddenly switched to its minimum value ($-\ddot{\theta}$) at a suitable switching time (t_s). Please note that the blend points are always symmetric about the halfway point in time. Maximum acceleration is selected only if the blend points meet at the half point. In other words, it is obtained when t_s is equal to half of the operation time (t_f). Therefore, the maximum acceleration can be written as

$$\ddot{\theta}_{max} = \frac{4(\theta_f - \theta_0)}{t^2} \tag{3.42}$$

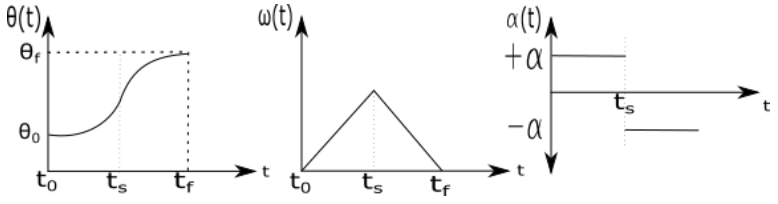

Figure 3.21. Position (left), velocity (middle), and acceleration (right) profiles for the minimum-time trajectory.

3.2.3. Control System

Control box of the manipulator is shown in Figure 3.22. It is composed of three HCS02.1E-W0012/CSH01.1C-S3-ENS-NNNN drivers for the manipulator, two HCS01.1E-W0009-A-02-B-ET-EC-NN-NN-NN-FW drivers for the 2-DOF gripper, and a INDRACONTROL MLC L45 controller. The manipulator is controlled with a PLC logic running in real-time mode. As a result, we have a functional control platform which is synchronized perfectly with the robot motion. The brand of the automation products is Rexroth Bosch Group. Technical specifications of the automation products are shown in Appendix D.

3.3. Performance Analyses

In this section, torque and speed characteristics of the manipulator for a given task are analytically analyzed for two cases: with the 2-DOF gripper vs. with a single gripper consisting of a vacuum holder to hold an object. There are three main factors that affect comparison of the two grippers. First of all, the single gripper consists of a stationary platform and a vacuum holder, which is 0.23 kg. On the other hand, overall mass of the 2-DOF gripper is 1.4 kg. Second, mass of the carried object (m) is doubled for 2-DOF gripper as two objects are carried at the same time. Finally, the number of (PnP) motion performed with the 2-DOF gripper is half of the one of the single gripper. These factors were considered for the analyses.

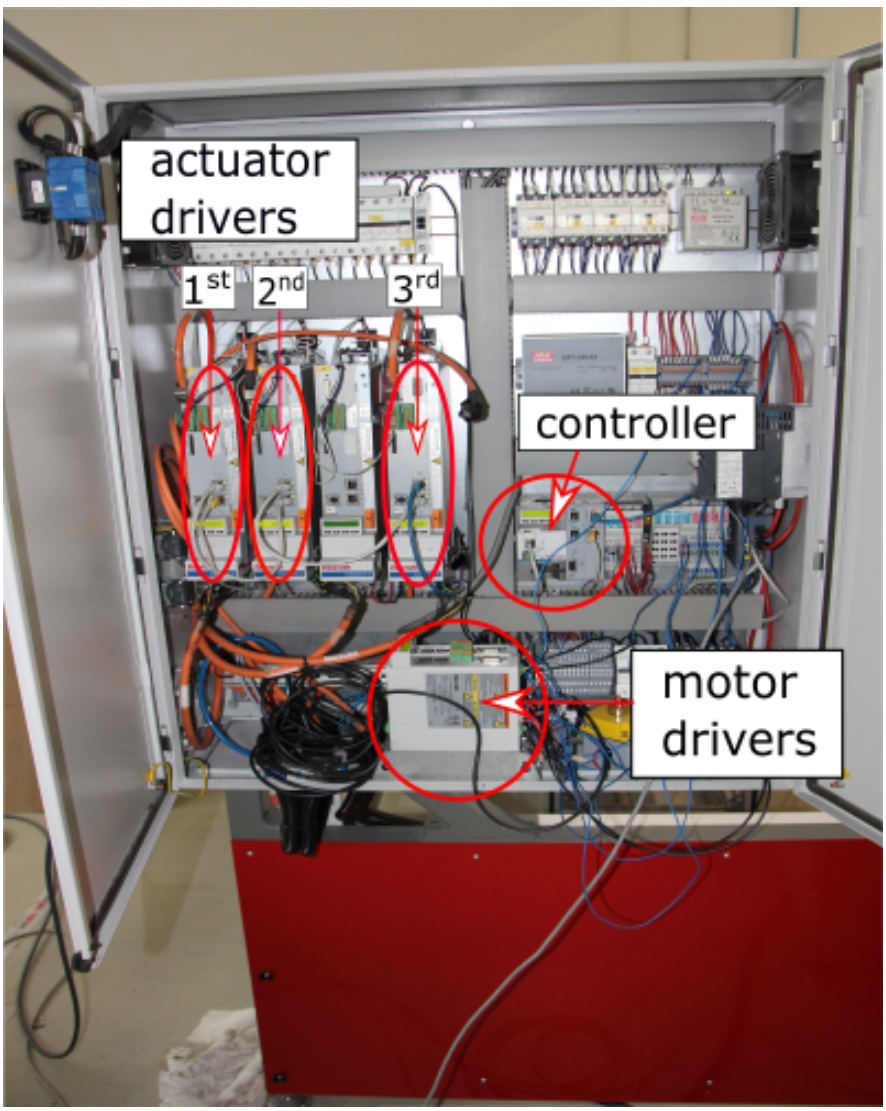

Figure 3.22. Control box of the manipulator.

There are two main performance criteria for the 2-DOF gripper. First, cycle time should be reduced compared to the single gripper. It is because cycle time optimization is vital for the robotic industry [43]. Since two objects are held at the same, only one PnP motion is performed with the proposed design instead of two for every two objects. Second, total energy consumption to complete a given task in a given cycle time should be reduced compared to the single gripper. In the following subsections, analysis methods are described for both performance criteria.

3.3.1. Cycle Time Reduction

Cycle time is defined as the time taken to complete a movement on a predefined path. For our analysis, cycle time is the duration to move the end effector from the initial to the final position on the benchmark path shown in Figure 3.18. In order to compare the single gripper and 2-DOF gripper in terms of cycle time, the benchmark path was quantified based on the standard practice in the literature [44] such that the manipulator end effector travels up 25 mm, go across 305 mm, and travels down 25 mm. The manipulator was assumed to be operated at the highest speed possible and ultimately with the maximum acceleration indicated in Equation 3.42. Therefore, the lowest possible cycle times with the two grippers were calculated for the manipulator. The duration for each sub-path was equal to each other and taken as

$$t_{sub} = \frac{t_{cycle}}{3} = \sqrt{\frac{\theta_f - \theta_0}{\ddot{\theta}_{max}}}$$

Since the required actuator torques alter with respect to the manipulator configuration, cycle time was analyzed on eight different PnP paths in the workspace (see Figure 3.23). Note that the manipulator picks the objects at point 0, and places them at points indicated by Latin numbers I-VIII.

The procedure to determine the lowest cycle times is illustrated in Figure 3.24. First, the maximum actuator torque required to complete each PnP motion in a certain time was calculated using the dynamic equation of motion of the manipulator (Equation

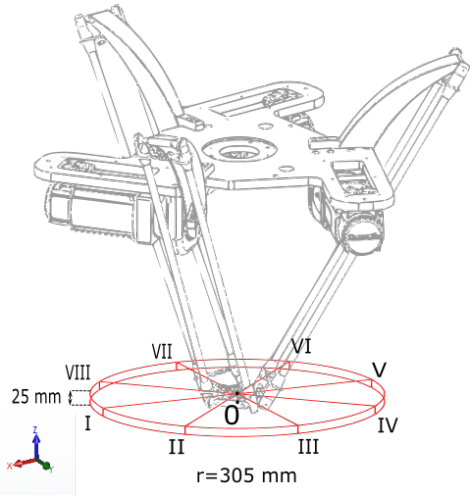

Figure 3.23. Eight paths followed by the manipulator for the cycle time analyses.

C.34-C.36). This step was repeated for nine different cycle times, evenly spaced in a range from $t_{cycle} = 0.3$ s to $t_{cycle} = 1.5$ s. Then, these maximum torques were plotted with respect to the corresponding angular speed of the actuator. This curve, which can be expressed by a quadratic equation, represents the load line of the manipulator [45]. Second, the characteristic torque-speed curve of the motors for continuous operation, which is linear, was drawn on the same plot. The intersection point of the torque-speed curve and the load line gave us the maximum operating speed of the actuators, and consequently, the lowest possible cycle time. This procedure was repeated for both grippers on each PnP path.

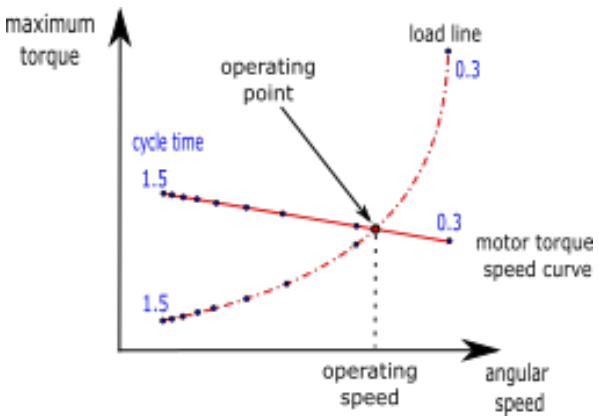

Figure 3.24. Procedure to find the lowest possible cycle time.

3.3.2. Energy Reduction

In this section, energy consumed by the manipulator for a given task is calculated for the single gripper and the 2-DOF gripper. For this purpose, a benchmark task, which requires to pick and place eight objects, was defined as follows. Eight objects, 7 grams coins, were assumed to be positioned on a conveyor (see Figure 3.25). The manipulator started from its zero position (see Figure 3.26). The objects were to be picked up in the order of numbers assigned to them, and placed in two target boxes. Geometric coordinates of the 4-pair objects are shown in Table 3.6. For the single gripper, the first four objects were placed in the first box and the remaining ones were placed in the second box. As for the 2-DOF gripper, the odd numbered objects were placed in the first box while the even numbered objects were placed in the second box. The single gripper made 8 PnP motions. On the other hand, the 2-DOF gripper made only 4 PnP motions since two objects were carried at once.

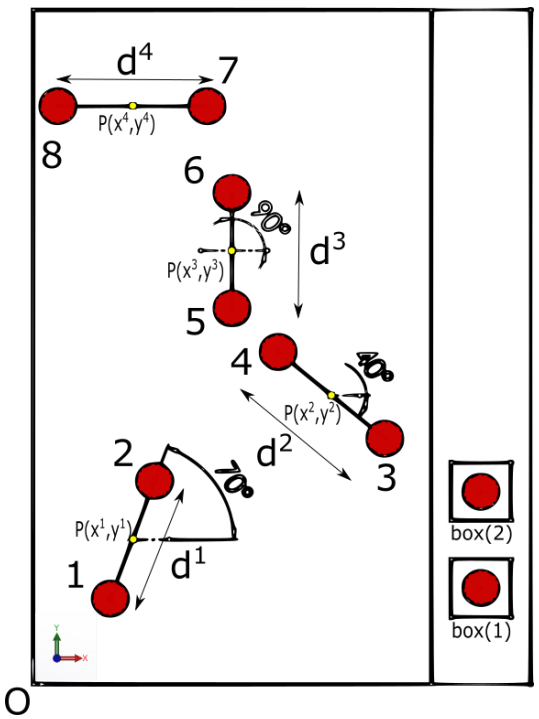

Figure 3.25. Benchmark test setup. 8 objects placed on a conveyor are to be collected.

The manipulator follows the benchmark path described in Figure 3.18 for each PnP motion. First of all, the manipulator travels up 25 mm in z-axis after picking the

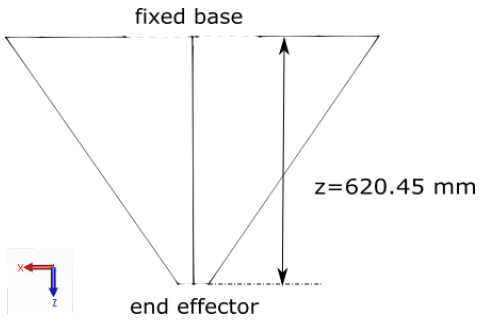

Figure 3.26. Zero position of the manipulator.

Table 3.6. Poses of the 4-pair objects.

i	x^i (mm)	y^i (mm)	d^i (mm)	θ^i (deg)
1	50	75	65	70
2	150	150	70	-40
3	100	225	60	90
4	50	300	75	0

objects. Second, it goes across on the xy plane and reaches above the corresponding boxes. The objects are positioned on the conveyor in a way that traveling distance on the xy plane varies for the each object. Finally, the manipulator travels down 25 mm and places the objects. The minimum-time trajectory shown in Figure 3.21 was adapted for each sub-path.

In the analysis, required torque (T) and power (P) values were calculated for the manipulator to complete the operation with the single gripper and the 2-DOF gripper. It was again assumed that duration was the same for each sub-path, which was selected to be a reasonable value $t_{sub} = 0.4$ s. Therefore, the manipulator completed a PnP motion in 2.4 s. Total operation time was 9.6 s for the 2-DOF gripper and 19.2 s for the single gripper.

3.4. Performance Measurements

The pictures of the single gripper and the 2-DOF gripper integrated to the manipulator are shown in Figure 3.27. In this section, performance evaluation of the 2-DOF gripper is discussed. The manipulator was tested against the performance criteria (cycle time and energy consumption) to check whether experimental results were in line with the analyses. Both tests were repeated with each gripper. Position, speed, and the torque values of the actuators of the manipulator were taken with a sample rate of 250 Hz.

Figure 3.27. The single gripper (left), and the 2-DOF gripper (right) are integrated into the Delta-type manipulator.

3.4.1. Cycle Time Experiments

Cycle time was experimentally determined when the manipulator was programmed to follow the eight paths described in Figure 3.23. For each path (from I to VIII), the manipulator was run from the starting the point O, and made back and forth motions without any break. Therefore, cycle time was determined by dividing the total operation time by 16. This continuous motion was first made with the single gripper. After collecting the required data, the single gripper was removed from the manipulator and the 2-DOF gripper was mounted instead. Then, the same motion was repeated with the 2-DOF gripper. In this experiment, the manipulator was operated at the highest speed possible to find the lowest cycle time for both grippers.

3.4.2. Energy Consumption Experiments

The setup for the energy consumption experiment is shown in Figure 3.28. Eight coins were placed on a surface based on the benchmark test illustrated in Figure 3.25. First, the coins were picked up and placed to the boxes with the single gripper. Then, the 2-DOF gripper was mounted on the manipulator and the test was repeated. In this experiment, the manipulator was run at the same speed with both grippers to compare the total energy consumption properly.

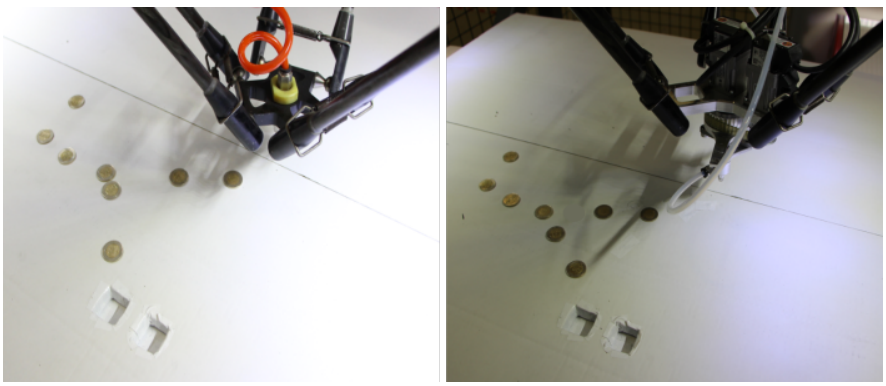

Figure 3.28. Eight coins are to be collected and placed to the target holes with the single gripper (left), and the 2-DOF gripper (right).

4. RESULTS

4.1. Technical Specifications

4.1.1. Workspace

Workspace of the 2-DOF gripper forms a hollow shape shown in Figure 4.1. Diameter of the inner is the minimum stroke of the slider-crank mechanism which is 50 mm. It was expected to be 20 mm. However, it could not be achieved to this value due to geometric constraints of the 2-DOF gripper such as thickness of the carriages. On the other hand, diameter of the outer circle is the maximum stroke of the slider-crank mechanism which is 140 mm. Therefore, the 2-DOF gripper is capable of holding two objects if their center distance is between 50 mm and 140 mm.

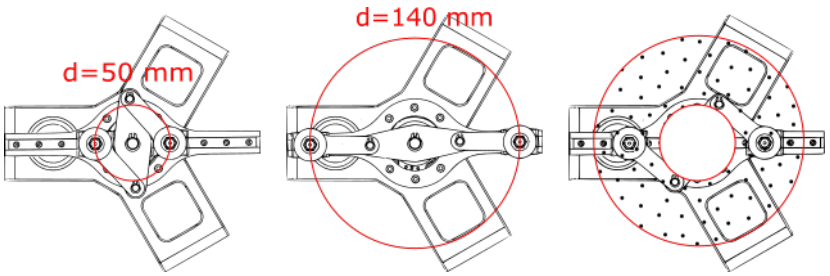

Figure 4.1. Workpace of the 2-DOF gripper. (Left) Minimum stroke of the slider-crank mechanism. (Middle) Maximum stroke of the slider-crank mechanism. (Right) Workspace is the area between the minimum and maximum strokes .

4.1.2. Speed

Following the methods described in Section 3.1.8.1, speed tests of the 2-DOF gripper were performed for translational and rotational motion. Position, speed, and the torque values of the motors were taken with a sample rate of 1 kHz. The results of the translational motion test are shown in Figure 4.2. It indicates that the motion is performed in 0.86 s. Therefore, the motor (1b) can make one reciprocate motion

within the range of maximum and minimum stroke in 0.43 s. Therefore, speed of the translational motion is calculated as 418.6 mm/s. Moreover, the motor can reach up to 1000 rpm in 50 ms. The speed must be zero at the maximum and minimum stroke points. However, it is noted that the speed fluctuates a little due to the vibration effects. Moreover, it can be inferred from the torque vs time graph that the torque required is slightly decreased in the 2^{nd} reciprocating motion. It is because more torque is required to initiate the motion.

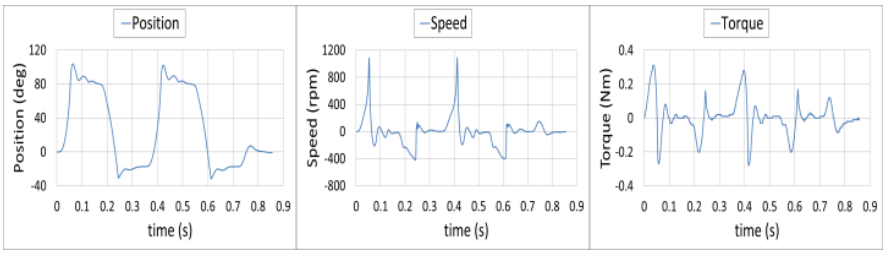

Figure 4.2. Position (left), speed (middle), and torque (right) of the motor (1b) of the 2-DOF gripper.

The results of the rotational motion test are shown in Figure 4.3. It indicates that the motion is performed in 1 s. Therefore, the motor (1a) is capable of performing 90° rotation in 0.25 s. Therefore, speed of the rotational motion is calculated as 60 rpm. Moreover, the motor can reach up to 600 rpm in 80 ms. The speed must be zero at the beginning and at the end of the each 90° rotation. However, it is again noted that the speed fluctuates around zero. It is because vacuum holders slides along the rail. Therefore, this results in position error and the motor tries to compensate it.

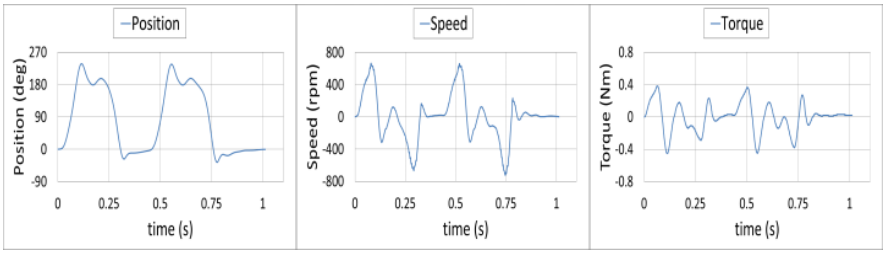

Figure 4.3. Position (left), speed (middle), and torque (right) of the motor (1a) of the 2-DOF gripper.

4.1.3. Position Sensing

Accuracy of the motor (MSM019A-0300) is 120 angular second, which is 0.033°. Therefore, position error of the stroke (referred to Equation 3.37) for a full cycle is shown in Figure 4.4. Moreover, position error for rotational motion is calculated as 0.0165°.

Figure 4.4. Position error of the stroke for a full motor cycle.

4.1.4. Repeatability and Accuracy

As it is mentioned in Section 3.1.8.3, repeatability test was performed. The results are shown in Figure 4.5. The mean and standard deviation of the stroke were calculated as 50.55 mm and 0.09 mm, respectively. To sum up, technical specifications of the 2-DOF gripper is illustrated in Table 4.1.

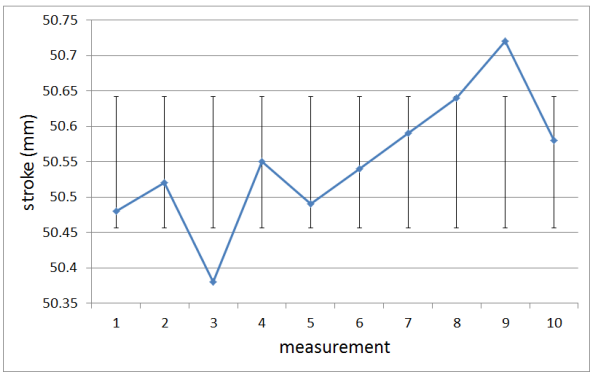

Figure 4.5. Repeatability test performed on the stroke with standart deviation.

Table 4.1. Technical specifications of the 2-DOF gripper.

Specification	**Property**	**Value**
workspace	hollow circle	50-140 mm
dimensions	height	175.8 mm
	width	170 mm
	depth	170 mm
total mass		1.4 kg
resolution	translational	<0.06 mm
	rotational	0.0165 deg
speed	tranlational	418.6 mm/s
	rotational	60 rpm

4.2. Results of Analyses

4.2.1. Cycle Time Analysis

Motor torque-speed curves and load lines for eight different paths are indicated in Figure 4.6. It can be inferred from the Figure 4.6 that when cycle time is decreased, the torque required is increased for both grippers. Moreover, it is noted that maximum torque values of the 2-DOF gripper are always greater than the single gripper for a given cycle time. This is an expected result because the 2-DOF gripper is heavier than the single gripper. Furthermore, the intersection points of the load lines and motor torque-speed curves give the lowest possible cycle times. If we normalize the cycle times by the number of objects carried, the cycle times are reduced to half for the 2-DOF gripper. It is because two objects are carried at once. The results are shown in Table 4.2. The average value was calculated by taking mean of the eight data. The cycle time of the single gripper is 0.448±0.07 s while the cycle time of the 2-DOF gripper is 0.268±0.08 s. On the other hand, the mean and the standard deviation of the cycle time reduction percentage are 40.33 and 8.54 respectively for the eight different paths.

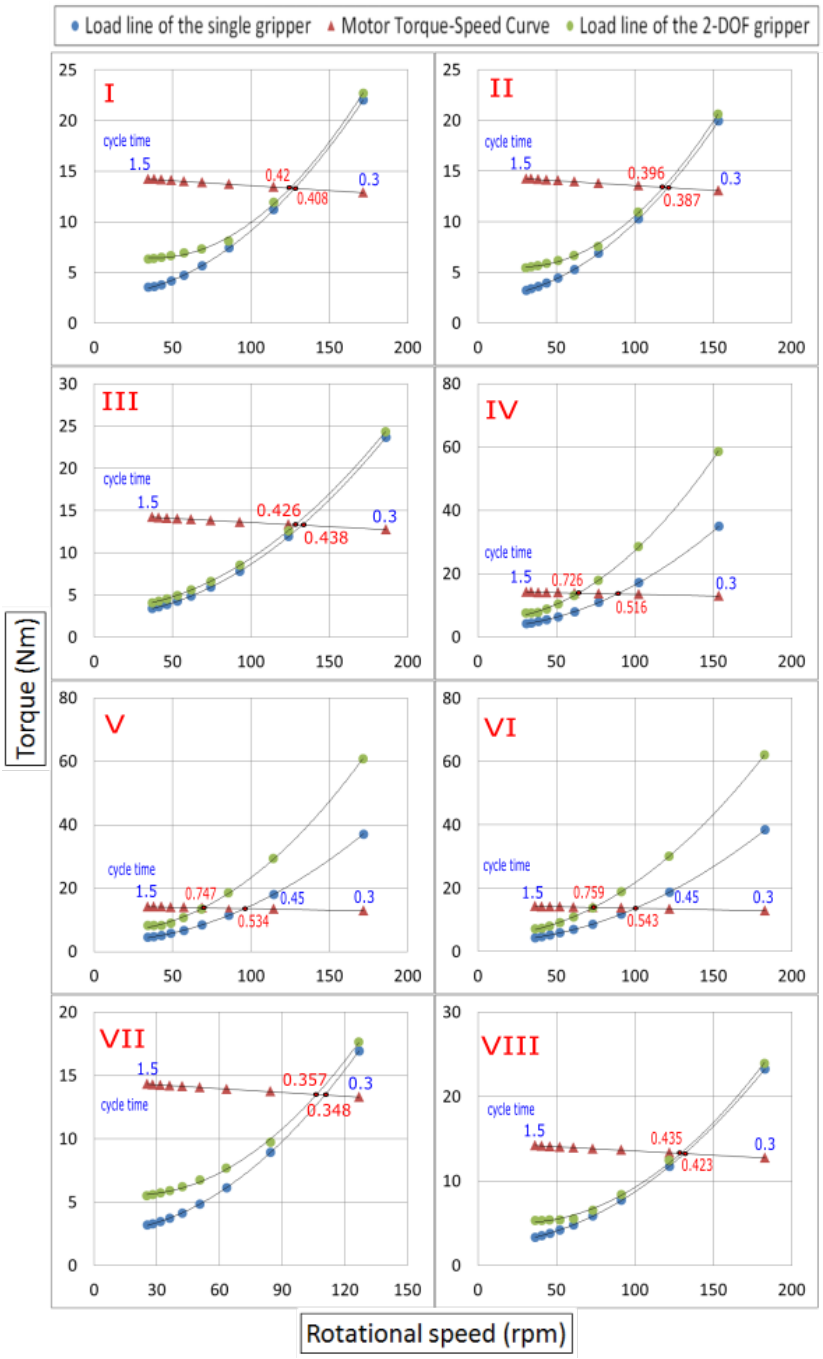

Figure 4.6. Load lines of the manipulator with the single gripper and the 2-DOF gripper, and motor torque-speed curves of the actuators of the manipulator.

Table 4.2. Cycle times on eight different paths with each gripper.

Path	**single gripper [s]**	**2-DOF gripper [s]**	**cycle time reduction [%]**
I	0.408	0.210	48.5
II	0.387	0.198	48.8
III	0.426	0.219	48.6
IV	0.516	0.363	29.7
V	0.534	0.374	30.1
VI	0.543	0.380	30.1
VII	0.348	0.179	48.7
VIII	0.423	0.218	48.6

4.2.2. Energy Reduction Analysis

Torque requirements for each actuator of the manipulator through the operation are shown in Figure 4.7. Please note that T_i and P_i for i= 1,2, and 3 represent torque and power values of the actuators of the manipulator. The results show that the maximum torque required for the task is higher with the 2-DOF gripper. This is an expected result because 2-DOF gripper is heavier than the single gripper and carries one more object. Moreover, power vs time graph is shown in Figure 4.8. It shows that power exerted by each actuator is different. However, it is not a clear graph to compare the 2-DOF gripper with the single gripper in terms of power requirement. Therefore, mean power required for picking and placing of each pair of objects is calculated to interpret the difference between the single gripper and the 2-DOF gripper. It is indicated in Figure 4.9 that the mean power is higher with the 2-DOF gripper. However, it is not twice higher than the one with the single gripper. Therefore, it is expected that total energy consumption during the operation should be less with the 2-DOF gripper because the total operation time is reduced by half with the 2-DOF gripper.

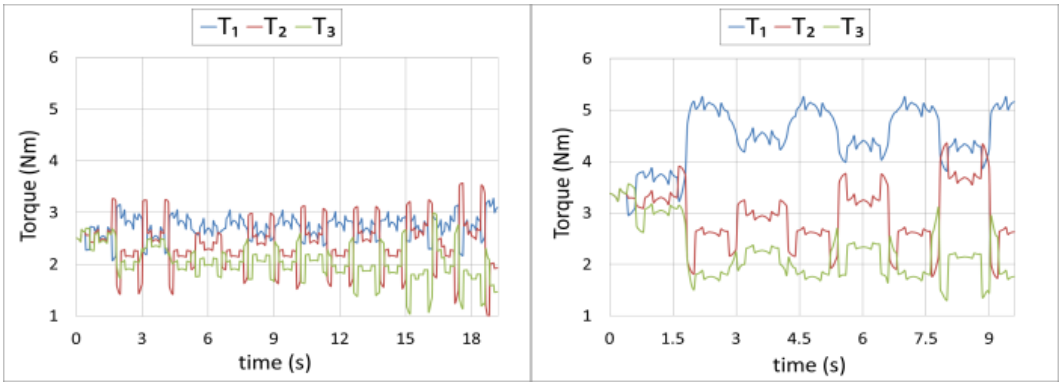

Figure 4.7. Torque vs time graph of the single gripper (left) and the 2-DOF gripper (right) for energy reduction analysis.

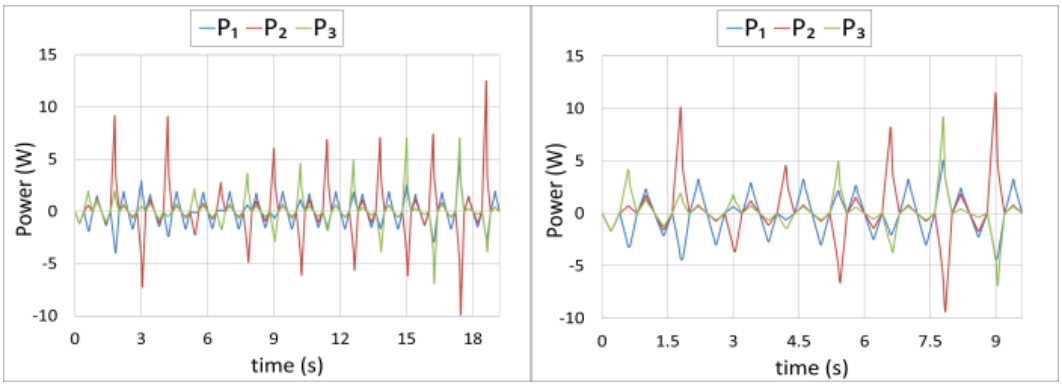

Figure 4.8. Power vs time graph of the single gripper (left) and the 2-DOF gripper (right) for energy reduction analysis.

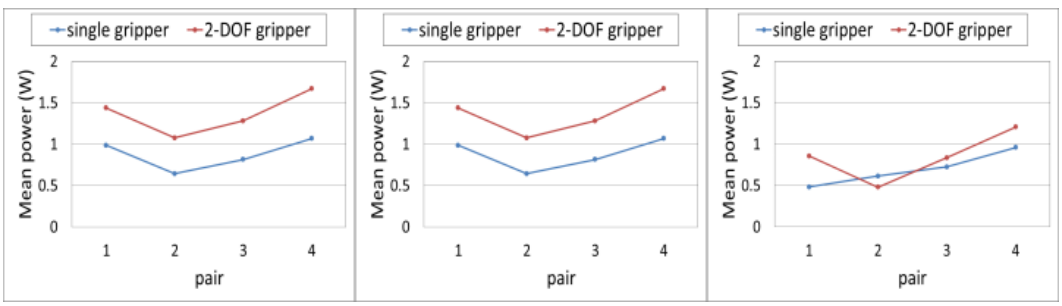

Figure 4.9. Mean power requirement for each actuator of the manipulator with the single gripper and the 2-DOF gripper. (Left) First actuator. (Middle) Second actuator. (Right) Third actuator.

The area under the power vs time graph gives the overall energy consumption. Total energy consumption with each gripper is shown in Figure 4.10. It indicates that the manipulator consumes less energy with the 2-DOF gripper. Energy reduction is 34.25% with the 2-DOF gripper for the benchmark operation.

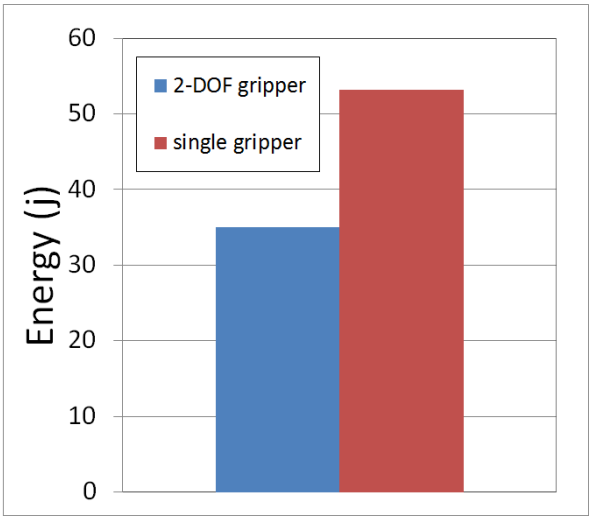

Figure 4.10. Total energy consumption of the manipulator during the operation with each gripper.

4.3. Measurement Results

4.3.1. Cycle Time Measurements

Total operation time was found 7.0 s and 9.4 s for the single gripper and the 2-DOF gripper respectively. It indicates that the cycle time of the single gripper is 0.438 s. Cycle time of the 2-DOF gripper is 0.294 s when normalized by the number of carried objects. Therefore, cycle time is decreased 32.9 percent with the 2-DOF gripper. Angular velocities of the actuators of the manipulator and a portion of the operation torque for both grippers are shown in Figure 4.11 and 4.12, respectively. They show that torque values under the maximum stall torque equation curve for continuous operation mode.

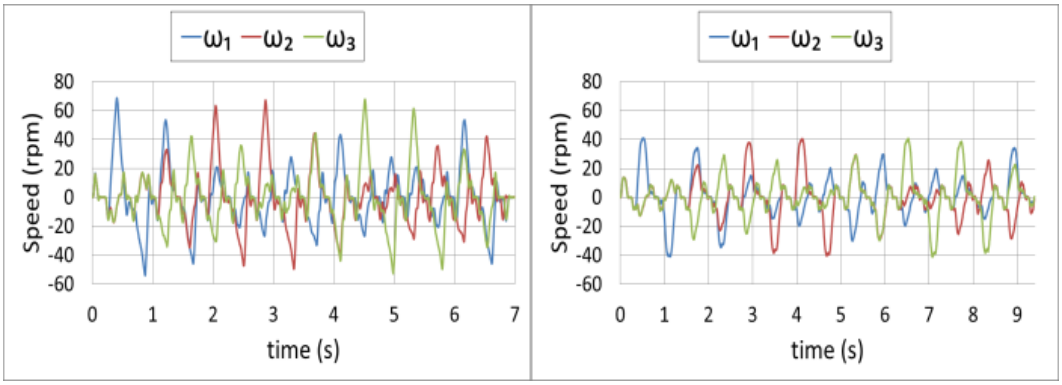

Figure 4.11. Angular speed of the manipulator with the single gripper (left) and the 2-DOF gripper (right).

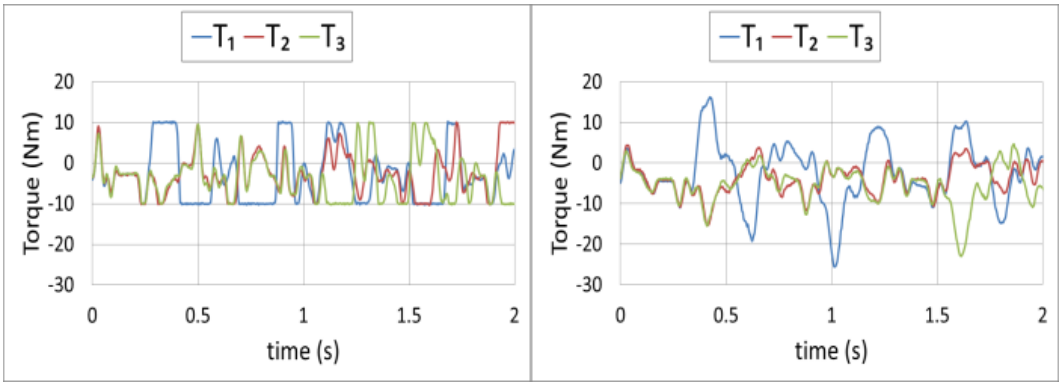

Figure 4.12. Torque requirement for the actuators of the manipulator with the single gripper (left) and the 2-DOF gripper (right).

4.3.2. Energy Reduction Measurements

Torque requirements for each actuator of the manipulator through the operation are shown in Figure 4.13. The results indicate that torque required for the task is higher with the 2-DOF gripper. It is due to the fact that 2-DOF gripper is heavier than the single gripper. Furthermore, torque requirements of the motors (1a) and (1b) are shown in Figure 4.14. It shows that torque requirements for the motors are very small compared to the actuators of the manipulator.

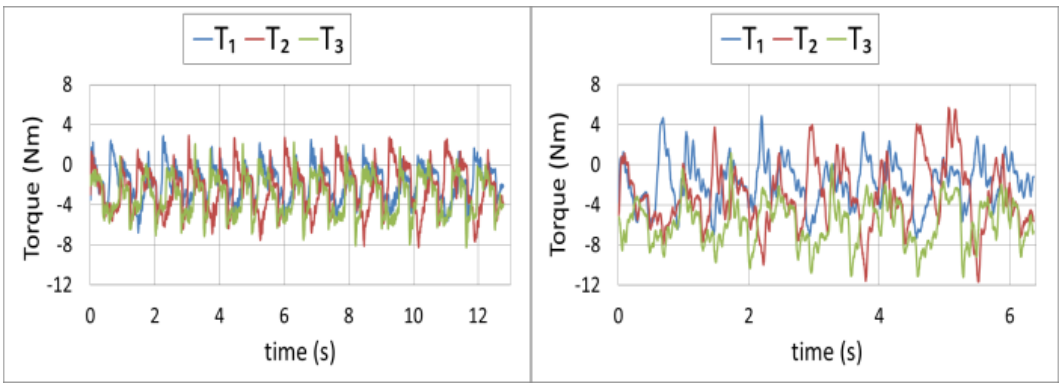

Figure 4.13. Torque vs time graph of the single gripper (left) and the 2-DOF gripper (right).

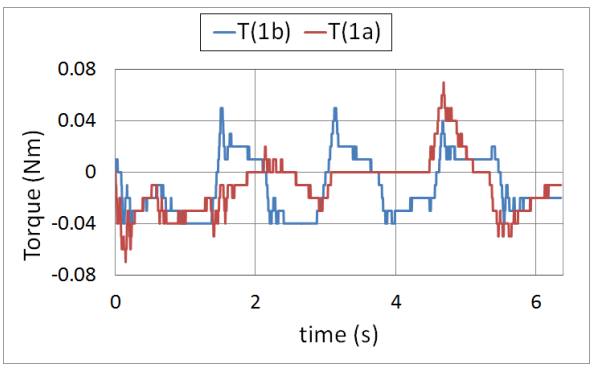

Figure 4.14. Torque vs time graph of the motors of the 2-DOF gripper.

It is noted that vacuum is activated while picking the objects and deactivated while placing them to the boxes. Positions for each actuator of the manipulator and vacuum activation are shown in Figure 4.15. 1 represents vacuum is on whereas 0 represents it is off.

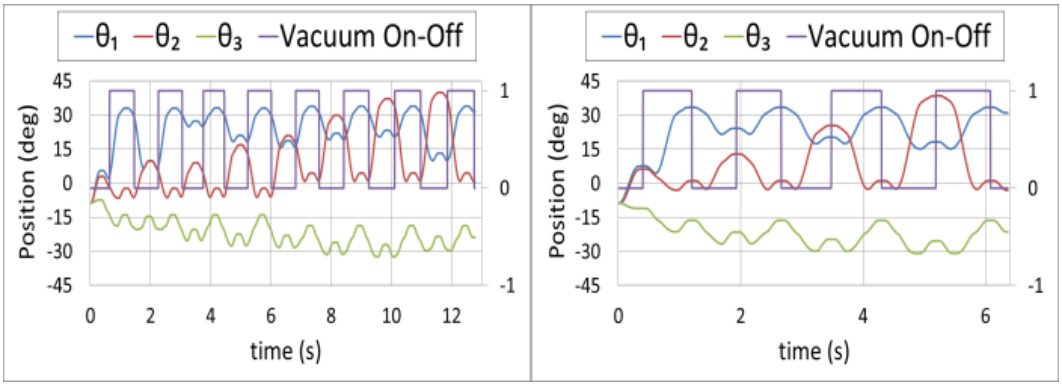

Figure 4.15. Positions of the actuators of the manipulator and vacuum activation. The single gripper (left) and the 2-DOF gripper (right).

Total energy consumption with each gripper together with actuators of the manipulator is shown in Figure 4.16. It demonstrates that energy is reduced 26.3% with the 2-DOF gripper for the benchmark operation.

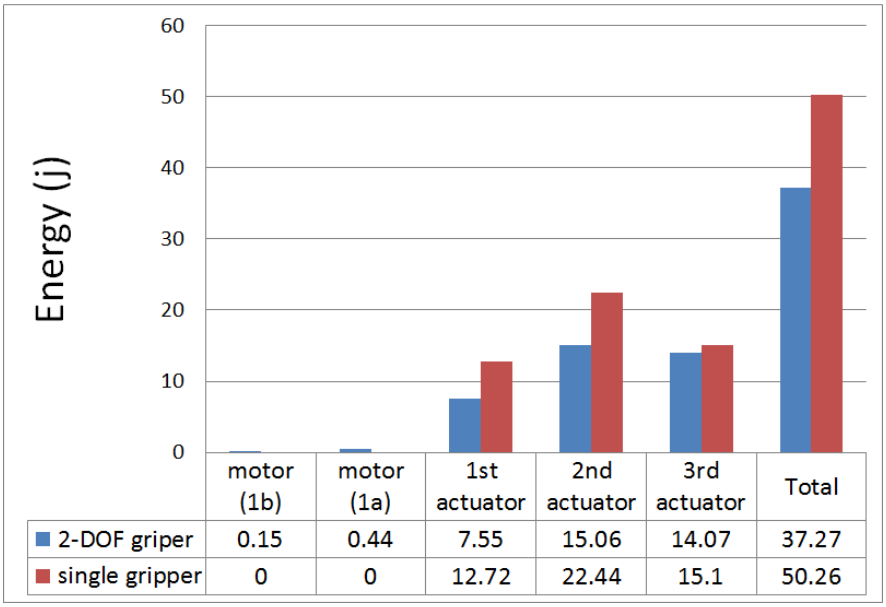

	motor (1b)	motor (1a)	1st actuator	2nd actuator	3rd actuator	Total
2-DOF griper	0.15	0.44	7.55	15.06	14.07	37.27
single gripper	0	0	12.72	22.44	15.1	50.26

Figure 4.16. Total energy consumption of the manipulator during the energy reduction test with each gripper.

5. DISCUSSIONS

As it is proposed earlier, the 2-DOF gripper, when integrated with an industrial robot, results in reduced cycle time and reduced energy consumption for a given task. It has been proved from the analyses and measurement results that the 2-DOF gripper satisfies the performance criteria. First of all, it has been showed that the 2-DOF gripper has advantages over the single gripper in terms of cycle time and energy consumption. Cycle time is reduced considerably with the 2-DOF gripper. Moreover, it is indicated in Figure 4.10 and Figure 4.16 that total energy consumption is decreased with the 2-DOF gripper. Second, it is noticed that the results of the measurements are partially consistent with the preliminary calculations. For instance, cycle time is reduced by 40.3 percent from the analyses whereas by 32.9 percent from the measurements. On the other hand, energy is reduced by 34.25 percent from the analyses whereas by 26.3 from the measurements. Note that the measurement results are eight percent less than the analyses results. The difference may be the result of mechanical and friction losses.

6. CONCLUSION

In this study, a novel two degree-of-freedom gripper for parallel manipulator has been designed and developed. The idea behind the study is picking up two randomly-arriving objects simultaneously. It is believed that cycle time and energy consumption of PnP operations may decrease if a novel gripper is designed. First of all, preliminary analyses were performed. The analyses results showed that the 2-DOF gripper has certain advantages over their counterparts used in PnP operations. Second, our design has been integrated with a 3-DOF parallel manipulator in order to see whether the gripper satisfies the performance criteria or not in a benchmark operation. Cycle time and energy reduction tests were performed with a single gripper and the 2-DOF gripper. The measurement results indicated that cycle time and total energy consumption for a given task are significantly reduced.

6.1. Contributions and Originality

The findings of the study will redound to the benefit of industry. It is due to the fact that the 2-DOF gripper, when integrated with a PM, will results in reduced cycle time and energy consumption.

A patent application based on the design of the 2-DOF gripper has been filed at the Turkish Patent Institute with no. 30059.13 2015/16277 under the name "ENDÜSTRİYEL ROBOTLAR İÇİN İKİ SERBESTLİK DERECELİ BİR TUTUCU SİSTEMİ". It is currently pending.

6.2. Outlook and Future Work

The novel 2-DOF gripper has certain benefits. However, it can be developed in many ways with further research and development. First of all, the overall mass of the 2-DOF gripper is 1.4 kg. It is a very heavy gripper for PnP operations. There are two ways to minimize it. One option is to employ lighter and stronger materials to the

design. In the manufacturing, aluminum 7075 is mostly used for components of the 2-DOF gripper. However, composite materials could be used too. Another option is to manufacture some of the purchased components. It is because geometric dimensions of them constraint the geometry of other components. For instance, outer diameter of the coupling were too much. Therefore, we are forced to use a bigger angular contact bearing and ultimately a larger pulley. Second, the 2-DOF gripper was tested with stationary objects with predefined positions. In the future, performance analysis can be performed with industrial image processing, which is based on cameras and other imaging components to detect positions of objects within a production line.

REFERENCES

1. Pettersson, A., S. Davis, J. Gray, T. Dodd and T. Ohlsson, "Design of a magnetorheological robot gripper for handling of delicate food products with varying shapes", *Journal of Food Engineering*, Vol. 98, No. 3, pp. 332–338, 2010.

2. Kumar, V., "Characterization of workspaces of parallel manipulators", *Journal of Mechanical Design*, Vol. 114, No. 3, pp. 368–375, 1992.

3. Meng, X., F. Gao, S. Wu and Q. J. Ge, "Type synthesis of parallel robotic mechanisms: Framework and brief review", *Mechanism and Machine Theory*, Vol. 78, pp. 177–186, 2014.

4. Brinker, J., B. Corves and M. Wahle, "A Comparative Study of Inverse Dynamics based on Clavel's Delta robot", *14th World Congress in Mechanism and Machine Science, Taipei*, 2015.

5. Xinjun, L., "Optimal kinematic design of a three translational DoFs parallel manipulator [J]", *Robotica*, Vol. 24, No. 2, pp. 239–250, 2006.

6. Patel, Y. and P. George, "Parallel manipulators applications—a survey", *Modern Mechanical Engineering*, Vol. 2, No. 03, p. 57, 2012.

7. Merlet, J.-P., *Parallel robots*, Vol. 74, Springer Science & Business Media, 2012.

8. Siciliano, B. and O. Khatib, *Springer Handbook of Robotics*, Springer Science & Business Media, 2008.

9. Isaksson, M., A. Eriksson, M. Watson, T. Brogårdh and S. Nahavandi, "A method for extending planar axis-symmetric parallel manipulators to spatial mechanisms", *Mechanism and Machine Theory*, Vol. 83, pp. 1–13, 2015.

10. Li, Y. and Q. Xu, "Kinematic analysis and design of a new 3-DOF translational parallel manipulator", *Journal of Mechanical Design*, Vol. 128, No. 4, pp. 729–737, 2006.

11. Laribi, M., L. Romdhane and S. Zeghloul, "Analysis and dimensional synthesis of the DELTA robot for a prescribed workspace", *Mechanism and Machine Theory*, Vol. 42, No. 7, pp. 859–870, 2007.

12. Isaksson, M., C. Gosselin and K. Marlow, "An introduction to utilising the redundancy of a kinematically redundant parallel manipulator to operate a gripper", *Mechanism and Machine Theory*, Vol. 101, pp. 50–59, 2016.

13. Kats, V. and E. Levner, "Cyclic scheduling in a robotic production line", *Journal of Scheduling*, Vol. 5, No. 1, pp. 23–41, 2002.

14. Monkman, G. J., S. Hesse, R. Steinmann and H. Schunk, *Robot Grippers*, John Wiley & Sons, 2007.

15. Derby, S. and C. Connolly, "ABB high-speed picking robots establish themselves in food packaging", *Industrial Robot: An International Journal*, Vol. 34, No. 4, pp. 281–284, 2007.

16. Reynolds, P., "One controller handles three delta robots", `http://www.packworld.com/controls/machine-control/one-controller-handles-three-delta-robots`, 2011, accessed at November 2016.

17. Belfiore, N. P. and E. Pennestrì, "An atlas of linkage-type robotic grippers", *Mechanism and Machine Theory*, Vol. 32, No. 7, pp. 811–833, 1997.

18. Hesse, S., *Grippers and their applications*, Festo, 1998.

19. Chen, F. Y., "Gripping mechanisms for industrial robots: an overview", *Mechanism and Machine Theory*, Vol. 17, No. 5, pp. 299–311, 1982.

20. EI-Kalay, A., M. Akyurt, A. Aljawi and F. Dehlawi, "On gripping mechanisms for industrial robots", Fourt Saudi Engineering Conferance, 1995.

21. Peer, A., S. Einenkel and M. Buss, "Multi-fingered telemanipulation-mapping of a human hand to a three finger gripper", *RO-MAN 2008-The 17th IEEE International Symposium on Robot and Human Interactive Communication*, pp. 465–470, IEEE, 2008.

22. Newman, W. S., B. B. Mathewson, Y. Zheng and S. Choi, "A novel selective-area gripper for layered assembly of laminated objects", *Robotics and Computer-Integrated Manufacturing*, Vol. 12, No. 4, pp. 293–302, 1996.

23. Micallef, R., "Overview of vacuum and gripper end effectors", *Robotics Engineering*, Vol. 8, No. 2, pp. 5–8, 1986.

24. Failli, F. and G. Dini, "An innovative approach to the automated stacking and grasping of leather plies", *CIRP Annals-Manufacturing Technology*, Vol. 53, No. 1, pp. 31–34, 2004.

25. Mantriota, G., "Optimal grasp of vacuum grippers with multiple suction cups", *Mechanism and Machine Theory*, Vol. 42, No. 1, pp. 18–33, 2007.

26. Bernier, C., "Magnetic Robot End Effector: Top 5 Pros and Cons", `http://blog.robotiq.com/bid/65794/Magnetic-Robot-End-Effector-Top-5-Pros-and-Cons`, 2014, accessed at December 2016.

27. Amend, J. R., E. Brown, N. Rodenberg, H. M. Jaeger and H. Lipson, "A positive pressure universal gripper based on the jamming of granular material", *IEEE Transactions on Robotics*, Vol. 28, No. 2, pp. 341–350, 2012.

28. Reddy, P. V. P. and V. Suresh, "A review on importance of universal gripper in industrial robot applications", *Int. J. Mech. Eng. Robot. Res*, Vol. 2, No. 2, pp. 255–264, 2013.

29. Jain, A. K., *Fundamentals of digital image processing*, Prentice-Hall, Inc., 1989.

30. Chen, Y., Y. Sun and C. Chen, "Dynamic analysis of a planar slider-crank mechanism with clearance for a high speed and heavy load press system", *Mechanism and Machine Theory*, Vol. 98, pp. 81–100, 2016.

31. Stojanovic, B., S. Tanasijevic and N. Miloradovic, "Tribomechanical systems in timing belt drives", *Journal of the Balkan Tribological Association*, Vol. 15, No. 4, pp. 465–473, 2009.

32. Callegari, M., F. Cannella and G. Ferri, "Multi-body modelling of timing belt dynamics", *Proceedings of the Institution of Mechanical Engineers, Part K: Journal of Multi-body Dynamics*, Vol. 217, No. 1, pp. 63–75, 2003.

33. Söylemez, E., *Mechanisms*, Middle East Technical University, 2013.

34. Baruh, H., *Analytical dynamics*, WCB/McGraw-Hill Boston, 1999.

35. Culpepper, M., "Elements of Mechanical Design", MIT open courseware, 2009.

36. Balli, S. S. and S. Chand, "Transmission angle in mechanisms (Triangle in mech)", *Mechanism and Machine Theory*, Vol. 37, No. 2, pp. 175–195, 2002.

37. Tao, D. C., *Applied linkage synthesis*, Addison-Wesley Pub. Co., 1964.

38. Clavel, R., "Dispositif pour le déplacement et le positionnement d'un élément dans l'espace", *Swiss patent*, , No. 672089A5, 1985.

39. Tsai, L.-W., G. C. Walsh and R. E. Stamper, "Kinematics of a novel three DOF translational platform", *Robotics and Automation, 1996. Proceedings., 1996 IEEE International Conference on*, Vol. 4, pp. 3446–3451, IEEE, 1996.

40. Tsai, L.-W., *Robot analysis: the mechanics of serial and parallel manipulators*, John Wiley & Sons, 1999.

41. Craig, J. J., *Introduction to robotics: mechanics and control*, Vol. 3, Pearson Prentice Hall Upper Saddle River, 2005.

42. Spong, M. W., S. Hutchinson and M. Vidyasagar, *Robot modeling and control*, Vol. 3, Wiley New York, 2006.

43. Borangiu, T., "Advances in Robot Design and Intelligent Control: Proceedings of the 24th International Conference on Robotics in Alpe-Adria-Danube Region (RAAD)", Vol. 371, 2015.

44. Wu, G., S. Bai and P. Hjørnet, "Architecture optimization of a parallel Schönflies-motion robot for pick-and-place applications in a predefined workspace", *Mechanism and Machine Theory*, Vol. 106, pp. 148–165, 2016.

45. Alciatore, D. G., *Introduction to mechatronics and measurement systems*, Tata McGraw-Hill Education, 2007.

46. Lagrange, J. L., *Mécanique analytique*, Vol. 1, Mallet-Bachelier, 1853.

APPENDIX A: DATASHEETS

Electrical data

Type	Maximumspeed n_{Max} [1/min]	Standstill torque M_0 [Nm]	Maximumtorque M_{Max} [Nm]	Maximum current I_{Max} [A]	Momentof inertia J [kgm²]
MSM019A-0300	5,000	0.16	0.48	3.3	0.000003
MSM019B-0300		0.32	0.95		0.000005
MSM031B-0300		0.64	1.91	4.9	0.000014
MSM031C-0300		1.3	3.8	7.7	0.000026
MSM041B-0300	4,500	2.4	7.1	12	0.000087

Figure A.1. Technical data of MSM019A-300 motor.

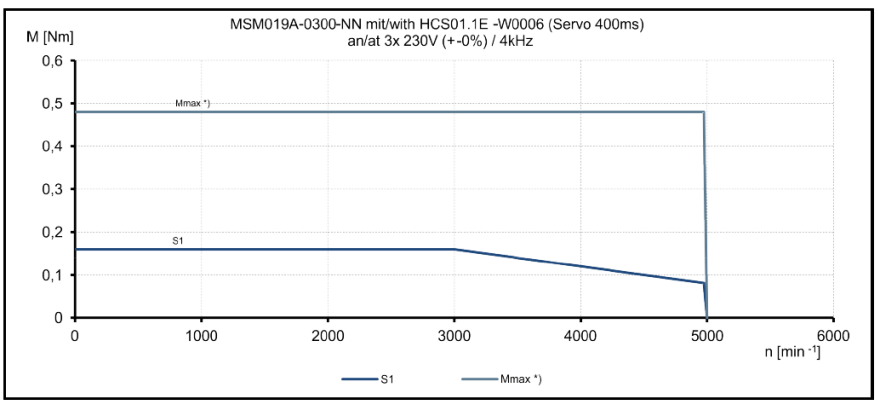

Figure A.2. Torque-speed characteristic of MSM019A-300 motor.

APPENDIX B: TECHNICAL DRAWINGS

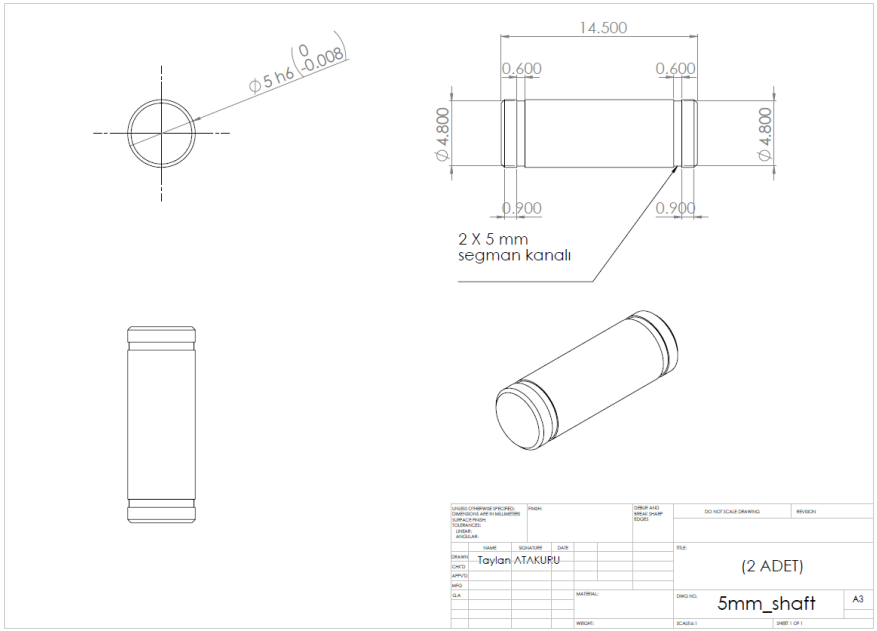

Figure B.1. Technical drawing of the 5 mm shaft.

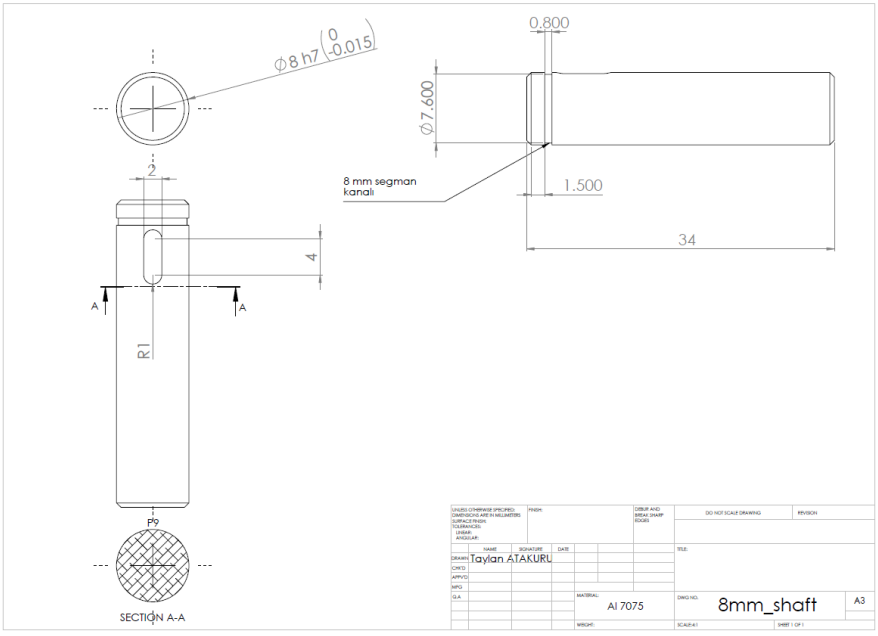

Figure B.2. Technical drawing of the 8 mm shaft.

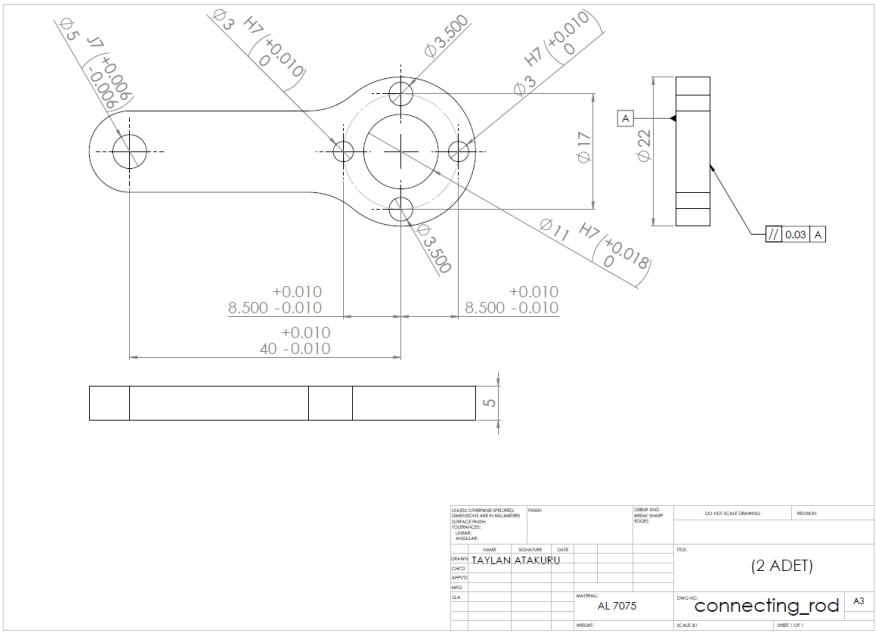

Figure B.3. Technical drawing of the connecting rod of the slider-crank mechanism.

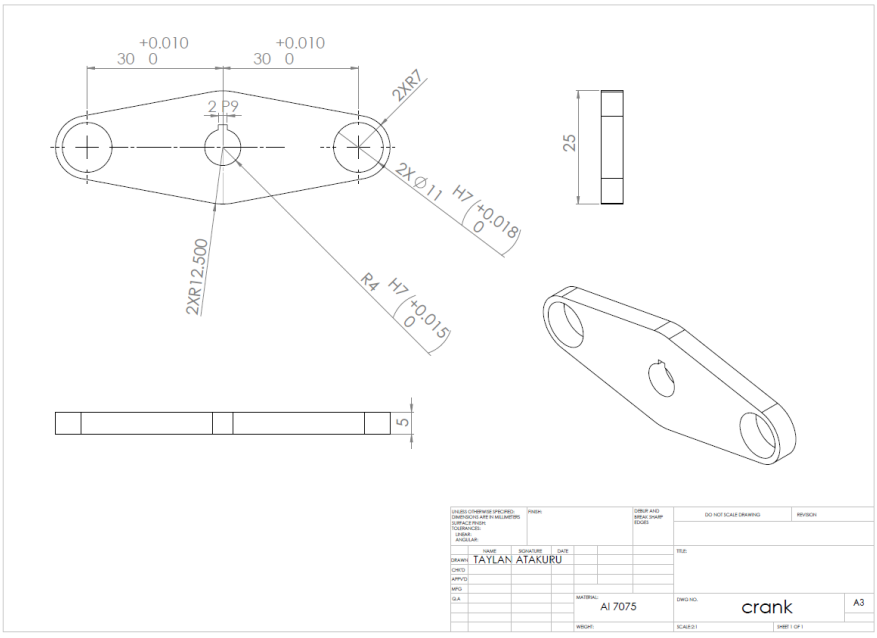

Figure B.4. Technical drawing of the crank of the slider-crank mechanism.

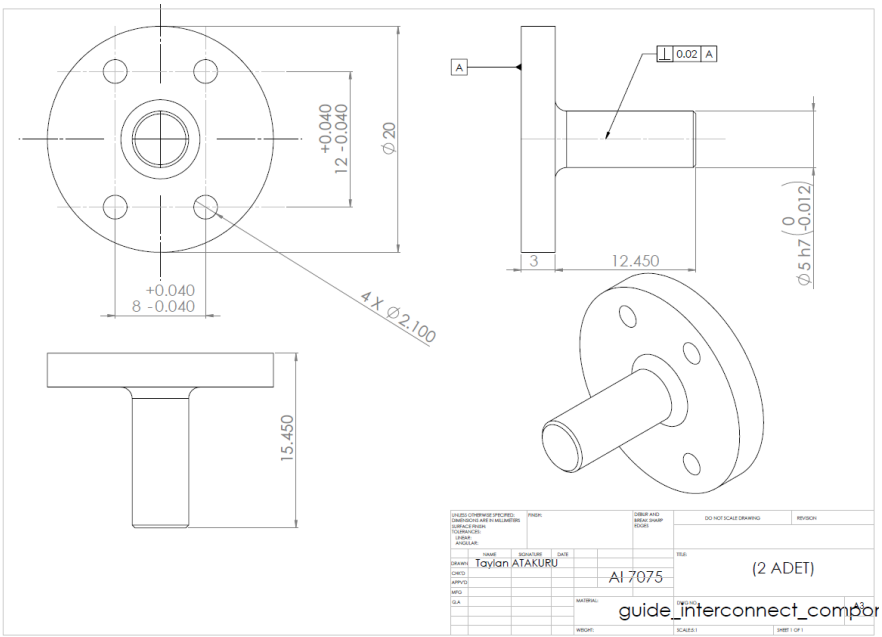

Figure B.5. Technical drawing of the guide connection component.

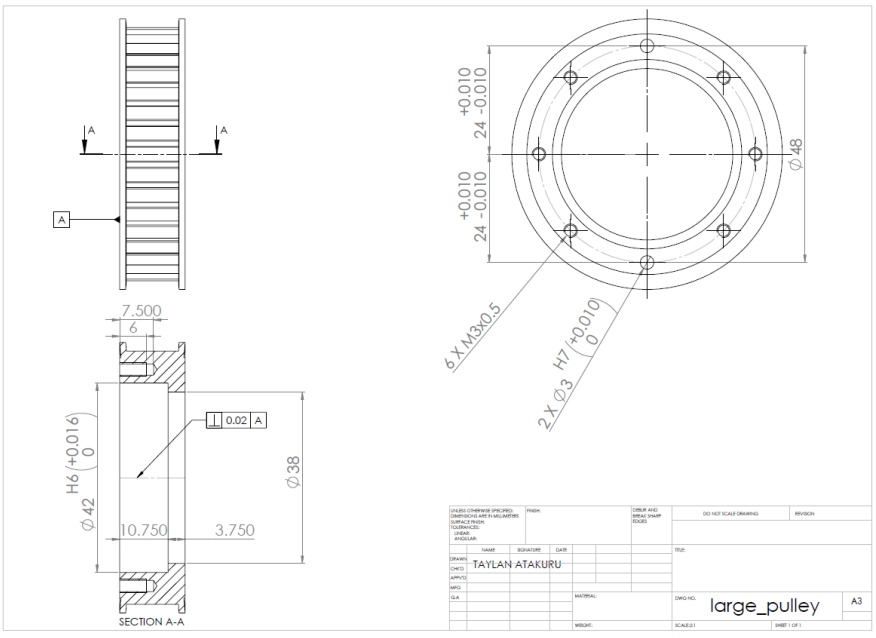

Figure B.6. Technical drawing of the large pulley of the timing belt pulley system.

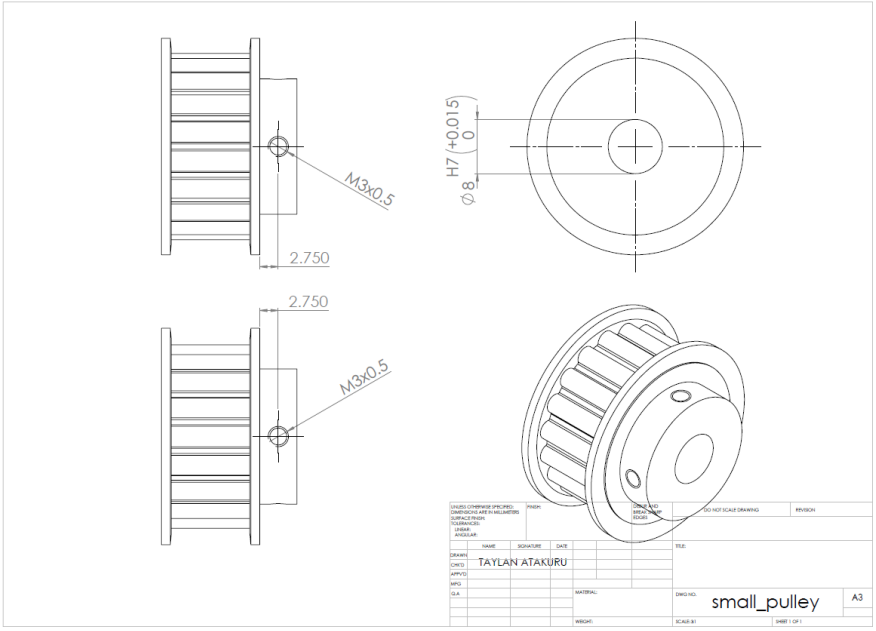

Figure B.7. Technical drawing of the small pulley of the timing belt pulley system.

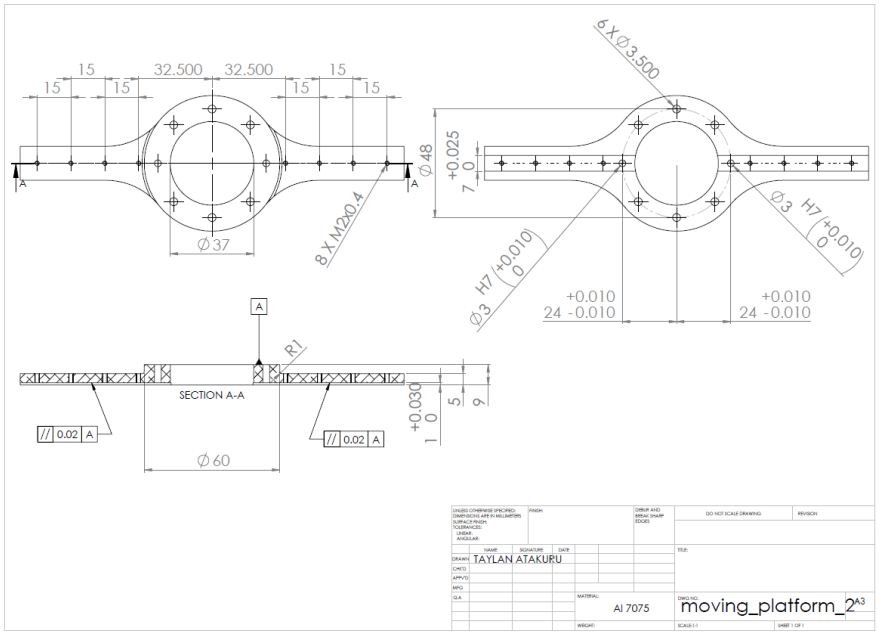

Figure B.8. Technical drawing of the moving platform.

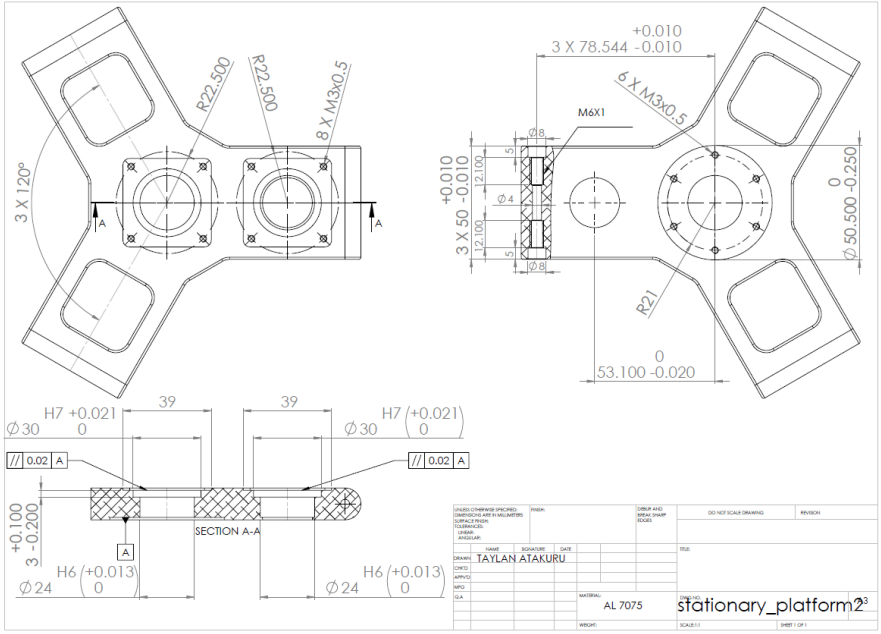

Figure B.9. Technical drawing of the stationary platform.

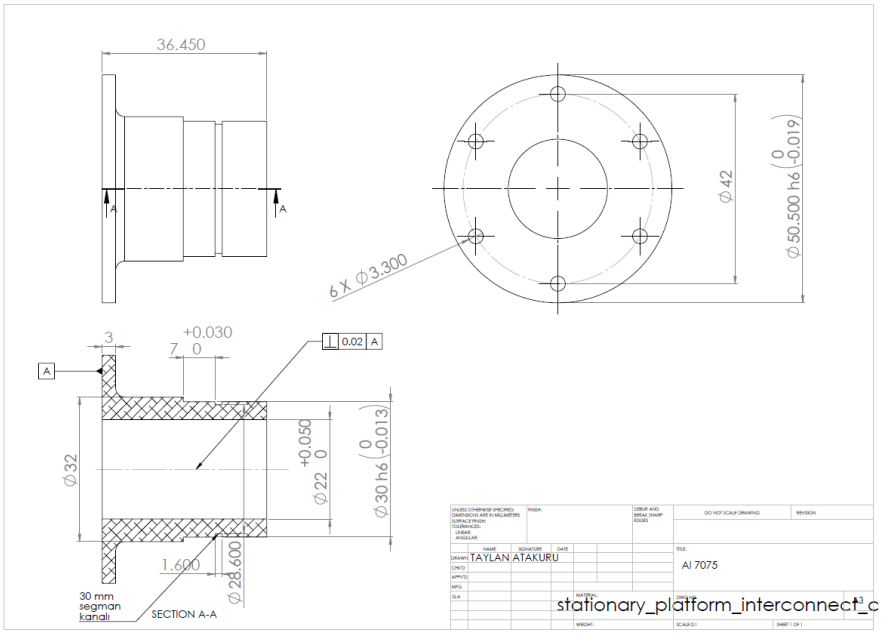

Figure B.10. Technical drawing of the stationary platform connection component.

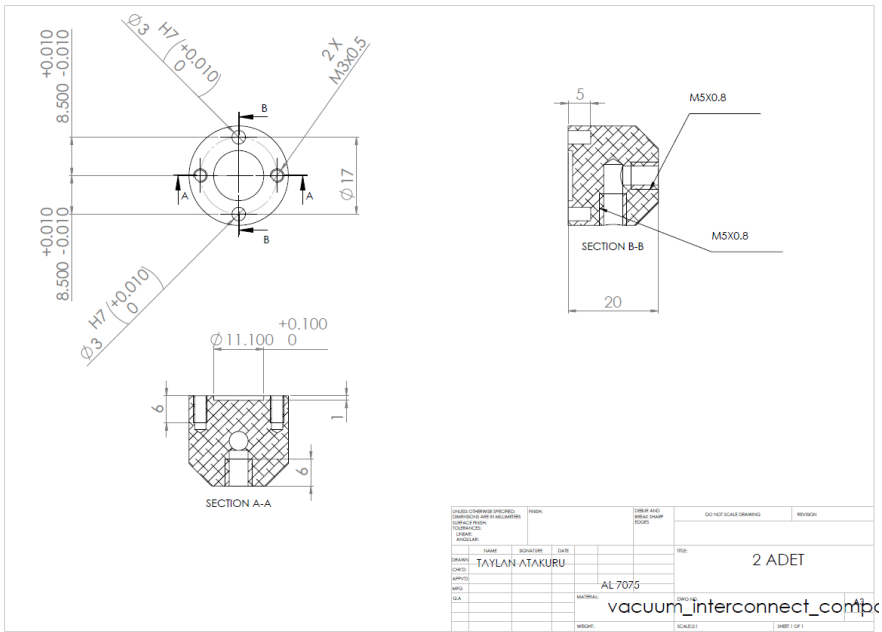

Figure B.11. Technical drawing of the vacuum connection component.

APPENDIX C: ROBOT ANALYSIS OF A DELTA MANIPULATOR

C.1. Geometry

As shown in Figure 3.17, there are two coordinate systems on the base. A reference coordinate system (x, y, z) and another coordinate system (x_i, y_i, z_i) are attached to the center point of the fixed base and the point A_i respectively.

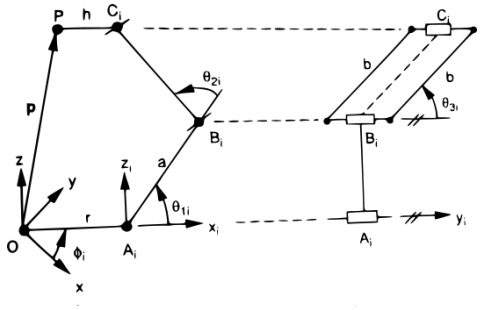

Figure C.1. Schematic drawing of a limb. Reprinted from [40].

Figure C.1 describes joint angles of the manipulator; θ_{1i} is measured from x_i axis to A_iB_i, θ_{2i} is the angle between the extended line of AB and B_iC_i, and θ_{3i} is measured from y_i axis to B_iC_i. In total, there are nine joint angles θ_{1i}, θ_{2i}, and θ_{3i} for $i = 1$, 2, and 3. θ_{1i}'s are considered as the actuated joints for each limb and a loop-closure equation can be written as:

$$\vec{A_iB_i} + \vec{B_iC_i} = \vec{OP} + \vec{PC_i} - \vec{OA_i} \tag{C.1}$$

Expressing Equation. C.1 in the (x_i, y_i, z_i) coordinate frame, it is obtained that

$$\begin{bmatrix} acos\theta_{1i} + bsin\theta_{3i}cos(\theta_{1i} + \theta_{2i}) \\ bcos\theta_{3i} \\ asin\theta_{1i} + bsin\theta_{3i}sin(\theta_{1i} + \theta_{2i}) \end{bmatrix} = \begin{bmatrix} c_{xi} \\ c_{yi} \\ c_{zi} \end{bmatrix} \tag{C.2}$$

where

$$\begin{bmatrix} c_{xi} \\ c_{yi} \\ c_{zi} \end{bmatrix} = \begin{bmatrix} cos\phi_i & sin\phi_i & 0 \\ -sin\phi_i & cos\phi_i & 0 \\ 0 & 0 & 1 \end{bmatrix} \begin{bmatrix} p_x \\ p_y \\ p_z \end{bmatrix} + \begin{bmatrix} h - r \\ 0 \\ 0 \end{bmatrix} \tag{C.3}$$

Equation C.3 expresses the position of point C_i relative to the (x_i,y_i,z_i) coordinate frame, wherein a and b are the lengths of lower and upper arms respectively, h=$|C_iP|$, r=$|OA_i|$ and P=$[p_x\ p_y\ p_z]^T$ is the position vector of point p relative to the (x, y, z) coordinate system.

C.2. Inverse Kinematics

Inverse kinematics is necessary to determine joint angles θ_{11}, θ_{12}, and θ_{13} that provide a desired position of moving platform. A geometric approach is used in order to find actuated joints [39]. It is obvious that once the position of point P is given, the position of point C_i can also be determined. It is considered that the surface generated by full range of motion of C_iB_i about point C forms a sphere centered at C_i and the full range of motion of A_iB_i forms a circle centered about A_i (see Figure C.2). The intersection of the sphere and the circle gives the solution of inverse kinematics. The possible cases: two solutions are obtained if the circle passes through the sphere, or one solution is obtained if the circle is tangent to the sphere, or no solution is obtained if the circle and the sphere do not intersect.

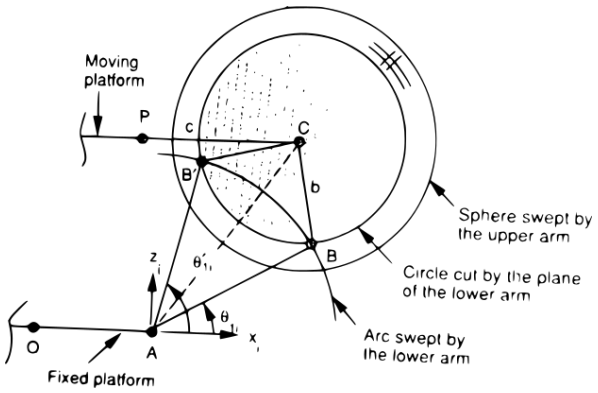

Figure C.2. Inverse kinematic solution of a limb. Reprinted from [40].

From the second row of Equation C.2, two solutions for θ_{3i} can be found as

$$\theta_{3i} = \mp cos^{-1}\frac{c_{yi}}{b} \tag{C.4}$$

Once θ_{3i} is selected, θ_{2i} can be found by summing the squares of the first and the third elements of Equation C.2, that is;

$$2absin\theta_{3i}cos\theta_{2i} + a^2 + b^2 = c_{xi}^2 + c_{yi}^2 + c_{zi}^2$$

Hence, θ_{2i} can be calculated as

$$\theta_{2i} = \mp cos^{-1}\left(\frac{c_{xi}^2 + c_{yi}^2 + c_{zi}^2 - a^2 - b^2}{2absin\theta_{3i}}\right) \tag{C.5}$$

Please note that Equation C.5 yields two solutions of θ_{2i}. Therefore, this results in four solution sets for θ_{2i} and θ_{3i}. Once θ_{2i} and θ_{3i} are found, θ_{1i} can be found by rearranging Equation C.2 as

$$bsin\theta_{3i}cos(\theta_{1i} + \theta_{2i}) = c_{xi} - acos\theta_{1i}bsin\theta_{3i}sin(\theta_{1i} + \theta_{2i}) = c_{zi} - asin\theta_{1i} \tag{C.6}$$

Summing the squares of Equation C.6, it is obtained

$$b^2 sin\theta_{3i}^2 = c_{xi}^2 + c_{zi}^2 + a^2 - 2a(c_{xi}cos\theta_{1i} + c_{zi}sin\theta_{1i}) \tag{C.7}$$

Let

$$D = \frac{c_{xi}^2 + c_{zi}^2 + a^2 - b^2 sin\theta_{3i}^2}{2a} = c_{xi}cos\theta_{1i} + c_{zi}sin\theta_{1i}$$

$$t = tan\frac{\theta_{1i}}{2}$$

Therefore,

$$sin\theta_{1i} = \frac{2t}{1+t^2} \qquad cos\theta_{1i} = \frac{1-t^2}{1+t^2} \tag{C.8}$$

Putting Equation C.8 into the Equation C.7, the term t can be calculated from this quadratic equation as

$$t_{1,2} = \frac{c_{zi} \pm \sqrt{c_{zi}^2 + c_{xi}^2 - D^2}}{c_{xi} + D} \tag{C.9}$$

Therefore, actuated joint angles θ_{1i} are calculated as

$$\theta_{1i} = 2\left[n\pi + tan^{-1}(\frac{c_{zi} + \sqrt{c_{zi}^2 + c_{xi}^2 - D^2}}{c_{xi} + D})\right] n = 0, 1, 2, ... \tag{C.10}$$

The inverse kinematics solution can be tested for special cases. If $|c_{yi}| < b$ and $|\kappa| < 1$,two solutions exist. If $|c_{yi}| = b$ and $c_{xi}^2 + c_{zi}^2 = a^2$, only one solution exists. If $|c_{yi}| > b$, no solution exists.

C.3. Direct Kinematics

The use of direct (or forward) kinematics is to compute the position of the moving platform from the input joint angles θ_{11}, θ_{12}, and θ_{13}. Again a geometric approach is used in order to find the position of the moving platform [39]. First of all, the surface composed of all possible positions of P for limb i with a given θ_{1i} creates a sphere centered at B_i', which is located h distance from the point B_i in the direction of C_iP. Second, when all three limbs is considered, the point P must fall on the three spheres created a sweep of P for each limb. Finally, the intersections of these three spheres give the solutions to the direct kinematics. There are four possible cases to be considered. First of all, two solutions exist at the intersections of the spheres. It is shown in Figure C.3. Second, one solution is obtained if one sphere is tangent to the circle of intersection of the other two spheres. Third, an infinite number of solutions are obtained if the centers of any two spheres coincide. It happens if and only if $\theta_{11} = \theta_{12} = \theta_{13} = \pi/2$ and $r = h$. Finally, no solution is obtained if the spheres do not intersect.

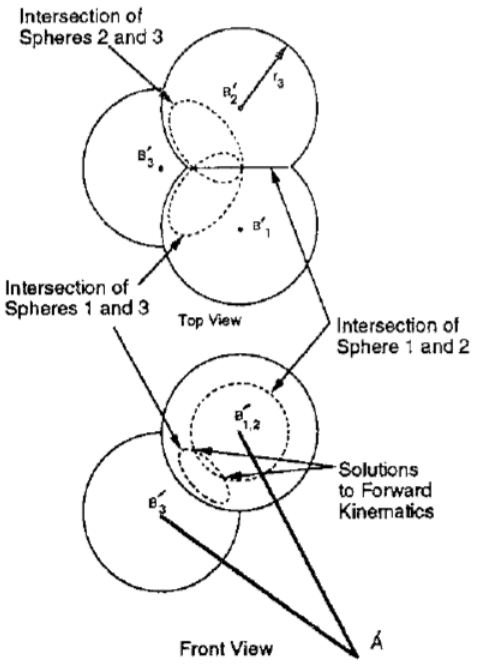

Figure C.3. Two forward kinematic solutions. Reprinted from [39].

The algebraic solution is obtained by writing the equations of the three spheres. When c_{xi}, c_{yi} and c_{zi} from Equation C.3 are substituted into Equation C.2 , it is obtained

$$\begin{bmatrix} bsin\theta_{3i}cos(\theta_{1i}+\theta_{2i}) \\ bcos\theta_{3i} \\ bsin\theta_{3i}sin(\theta_{1i}+\theta_{2i}) \end{bmatrix} = \begin{bmatrix} cos\phi_i & sin\phi_i & 0 \\ -sin\phi_i & cos\phi_i & 0 \\ 0 & 0 & 1 \end{bmatrix} \begin{bmatrix} p_x \\ p_y \\ p_z \end{bmatrix} + \begin{bmatrix} -acos\theta_{1i} - r + h \\ 0 \\ -asin\theta_{1i} \end{bmatrix} \tag{C.11}$$

By summing the squares of the three components of Equation C.11, an equation for the sphere swept by point P is obtained.

$$\begin{aligned} b^2 = {} & p_x^2 + p_y^2 + p_z^2 - 2(p_x cos\phi_i + p_y sin\phi_i)(acos\theta_{1i} + r - h) \\ & - 2p_z asin\theta_{1i} + (acos\theta_{1i} + r - h)^2 + a^2 sin^2\theta_{1i} \quad for \quad i = 1,\ 2,\ and\ 3 \end{aligned} \tag{C.12}$$

By subtracting Equation C.12 for $i = 1$ from Equation C.12 for $i = j$, the plane that contains the circle of intersection created by the spheres of limb 1 and limb j is found

$$e_{1j}p_x + e_{2j}p_y + e_{3j}p_z + e_{4j} = 0 \quad for \quad j = 2, 3 \tag{C.13}$$

where

$$e_{1j} = 2cos\phi_j(acos\theta_{1j} + r - h) - 2cos\phi_1(acos\theta_{11} + r - h)$$

$$e_{2j} = 2sin\phi_j(acos\theta_{1j} + r - h) - 2sin\phi_1(acos\theta_{11} + r - h)$$

$$e_{3j} = 2asin\theta_{1j} - 2asin\theta_{11}$$

$$e_{4j} = (acos\theta_{11} + r - h)^2 + a^2 sin^2\theta_{11} - (acos\theta_{1j} + r - h)^2 - a^2 sin^2\theta_{1j}$$

A system of two linearly independent equations is obtained by writing Equation C.13 twice for $j = 2$ and 3 as long as the centers of the spheres are not collinear. A line that contains point P is defined by this system of equations if there are real solutions. The direct kinematics is solved by intersecting this line with one of the spheres described by Equation C.12. Equation C.13 is solved for p_y and p_z in terms of p_x and then the resulting expressions is substituted into Equation C.12 for $i = 1$. It yields

$$k_0 p_x^2 + k_1 p_x + k_2 = 0 \tag{C.14}$$

The coefficients of the quadratic Equation C.14 are

$$k_0 = 1 + \frac{l_1^2}{l_2^2} + \frac{l_4^2}{l_2^2}$$

$$k_1 = \frac{2l_0 l_1}{l_2^2} + \frac{2l_3 l_4}{l_2^2} - 2l_5 cos\phi_1 - \frac{2l_5 l_1}{l_2} sin\phi_1 - \frac{2al_4}{l_2} sin\theta_{11}$$

$$k_2 = l_5^2 - b^2 + \frac{l_0^2}{l_2^2} + \frac{l_3^2}{l_2^2} + a^2 sin^2\theta_{11} - \frac{2l_0 l_5}{l_2} sin\phi_1 - \frac{2al_3}{l_2} sin\theta_{11}$$

where

$$l_0 = e_{32}e_{43} - e_{33}e_{42}$$

$$l_1 = e_{13}e_{32} - e_{12}e_{33}$$

$$l_2 = e_{22}e_{33} - e_{23}e_{32}$$

$$l_3 = e_{23}e_{42} - e_{22}e_{43}$$

$$l_4 = e_{12}e_{23} - e_{13}e_{22}$$

$$l_5 = acos\theta_{11} + r - h$$

where e_{12}, e_{13}, e_{22}, e_{23}, e_{32}, e_{33}, e_{42}, and e_{43} are the terms in Equation C.13. There are five possible cases to be considered.

(i) Generic solution. If $k_1^2 - 4k_0k_2 > 0$, two solutions exist in which the circle created by the intersection of two spheres intersects the third sphere in two places.

(ii) Singular solution. If $k_1^2 - 4k_0k_2 = 0$, the circle created by the intersection of two spheres is tangent to the third sphere, resulting in one real solution.

(iii) Singular solution. The centers of the spheres are collinear if the system of equations produced by Equation C.13 for j=2 and 3 are linearly independent. It results in an infinite number of solutions if the centers of the spheres are coincident.

(iv) No real solution. The centers of the spheres are collinear if the system of equations produced by Equation C.13 for $j = 2$ and 3 are linearly independent. It results in no solutions if the centers of the spheres are not coincident.

(v) No real solution. If $k_1^2 - 4k_0k_2 < 0$, the three spheres do not intersect and therefore, no real solutions exist.

Please note that once p_x is calculated, p_y and p_z values can be found by back substitution into Equation C.13.

$$e_{12}p_x + e_{22}p_y + e_{32}p_z + e_{42} = 0 \qquad for \quad j = 2 \tag{C.15}$$

$$e_{13}p_x + e_{23}p_y + e_{33}p_z + e_{43} = 0 \qquad for \quad j = 3 \tag{C.16}$$

When Equation C.15 and Equation C.16 are expressed in matrix form, it is obtained that

$$\begin{bmatrix} p_y \\ p_z \end{bmatrix} = \begin{bmatrix} e_{33} & e_{32} \\ e_{23} & e_{33} \end{bmatrix}^{-1} \begin{bmatrix} -e_{12}p_x - e_{42} \\ -e_{13}p_x - e_{43} \end{bmatrix} \tag{C.17}$$

Explicitly,

$$p_y = \frac{p_x(e_{13}e_{32} - e_{12}e_{33}) + e_{32}e_{43} - e_{42}e_{33}}{e_{22}e_{33} - e_{32}e_{43}} \tag{C.18}$$

$$p_z = \frac{p_x(e_{12}e_{23} - e_{22}e_{13}) + e_{42}e_{23} - e_{22}e_{43}}{e_{22}e_{33} - e_{32}e_{43}} \tag{C.19}$$

C.4. Jacobian Analyses

In this section, Jacobian matrix of the Maryland Manipulator is developed. By differentiating the loop-closure Equation C.1 with respect to time, it is obtained that

$$\vec{v}_p = \vec{\omega}_{1i} \times \vec{a}_i + \vec{\omega}_{2i} \times \vec{b}_i \tag{C.20}$$

where v_p is the linear velocity of the moving platform, $a_i = |A_iB_i|$, $b_i = |B_iC_i|$, ω_{ji} is the angular velocity of the j^{th} link of the i^{th} limb. Since the input vector is $\dot{q} = \begin{bmatrix} \dot{\theta}_{11} & \dot{\theta}_{12} & \dot{\theta}_{13} \end{bmatrix}^T$ for this manipulator, passive joint rates are eliminated by taking scalar product of both sides of Equation C.20 by b_i. It yields

$$\vec{b}_i \cdot \vec{v}_p = \vec{\omega}_{1i} \cdot (\vec{a}_i \times \vec{b}_i) \tag{C.21}$$

Expressing the vectors in Equation C.21 in the (x_i, y_i, z_i) coordinate frame, it is obtained

$$\mathbf{a_i^i} = a \begin{bmatrix} cos\theta_{1i} \\ 0 \\ sin\theta_{1i} \end{bmatrix}, \mathbf{b_i^i} = \begin{bmatrix} sin\theta_{3i}cos(\theta_{1i} + \theta_{2i}) \\ cos\theta_{3i} \\ sin\theta_{3i}sin(\theta_{1i} + \theta_{2i}) \end{bmatrix}$$

$$\omega_{\mathbf{1i}}^{\mathbf{i}} = \begin{bmatrix} 0 \\ -\dot{\theta}_{1i} \\ 0 \end{bmatrix}, \mathbf{v_p^i} = \begin{bmatrix} v_{p,x}cos\phi_i + v_{p,y}sin\phi_i \\ -v_{p,x}sin\phi_i + v_{p,y}cos\phi_i \\ v_{p,z} \end{bmatrix}$$

When the above expressions are substituted into Equation C.21, following results are obtained after some simplifications.

$$j_{ix}v_{p,x} + j_{iy}v_{p,x} + j_{iz}v_{p,z} = asin\theta_{2i}sin\theta_{3i}\dot{\theta}_{1i} \tag{C.22}$$

where

$$j_{ix} = cos(\theta_{1i} + \theta_{2i})sin\theta_{3i}cos\phi_i - cos_{3i}sin\phi_i$$

$$j_{iy} = cos(\theta_{1i} + \theta_{2i})sin\theta_{3i}sin\phi_i + cos_{3i}cos\phi_i$$

$$j_{iz} = sin(\theta_{1i} + \theta_{2i})sin\theta_{3i}$$

Please note that $j_i = [j_{ix}, j_{iy}, j_{iz}]^T$ represents a unit vector which is directed from B_i to C_i and it is expressed in the fixed (x, y, z) coordinate frame. Three scalar equations

are obtained by writing Equation C.22 three times, for i = 1,2, and 3. In matrix form,

$$J_x \mathbf{v_p} = J_q \dot{\mathbf{q}} \tag{C.23}$$

$$J_x = \begin{bmatrix} j_{1x} & j_{1y} & j_{1z} \\ j_{2x} & j_{2y} & j_{2z} \\ j_{3x} & j_{3y} & j_{3z} \end{bmatrix}, J_q = \begin{bmatrix} sin\theta_{21} sin\theta_{31} & 0 & 0 \\ 0 & sin\theta_{22} sin\theta_{32} & 0 \\ 0 & 0 & sin\theta_{23} sin\theta_{33} \end{bmatrix}$$

C.5. Lagrangian Dynamics

In this section, inverse dynamics of the Maryland Manipulator is solved by applying the Lagrangian equations of the first type [46] due to the complex kinematics of the manipulator. Therefore, a set of redundant coordinates are introduced in the Lagrangian equations of the first kind. However, the number of coordinates must be equal to number of equations so a set of constraint equations derived from the kinematics of the manipulator are required. The Lagrangian equations of the first type can be written as

$$\frac{d}{dt}(\frac{\partial L}{\partial \dot{q}_j}) - \frac{\partial L}{\partial q_j} = Q_j \sum_{i=1}^{k} \lambda_i \frac{\partial \Gamma_i}{\partial q_j} \quad for \quad j = 1 \; to \; n \tag{C.24}$$

where Γ_i represents i^{th} constraint function, k is the number of constraint equations, n is the number of generalized coordinates, and λ_i are the Lagrangian multipliers.

It is easier to solve the Lagrangian equation by dividing into two sets since the number of coordinates, n, exceeds the number of DOF by k. The first k-equation set contains the Lagrange multipliers. The second $n - k$ equation set, on the other hand, contains the generalized forces contributed by the actuators as the additional unknowns. The first set can be expressed in the form

$$\sum_{i=1}^{k} \lambda_i \frac{\partial \Gamma_i}{\partial q_j} = \frac{d}{dt}(\frac{\partial L}{\partial \dot{q}_j}) - \frac{\partial L}{\partial q_j} - \widehat{Q}_j \tag{C.25}$$

where $\widehat{Q}_j$ is the generalized force contributed by an external force, if any. Please note that since $\widehat{Q}_j$ is given in the inverse dynamics, the right hand side of Equation C.25 is known. Hence, the Lagrangian multipliers can be determined from a set of k linear equations. After the Lagrange multipliers are determined, the actuator torques and/or can be found from the remaining $n-k$ second set equations. It can be written as

$$Q_j = \frac{d}{dt}(\frac{\partial L}{\partial \dot{q}_j}) - \frac{\partial L}{\partial q_j} - \sum_{i=1}^{k} \lambda_i \frac{\partial \Gamma_i}{\partial q_j} \quad for \quad j = k+1 \; to \; n \tag{C.26}$$

where Q_j is the actuator torque or force.

As for Maryland manipulator, three redundant coordinates are introduced. These are the position of the moving platform in the Cartesian space, p_x, p_y, and p_z. Therefore, the manipulator has six generalized coordinates which are p_x, p_y, p_z, θ_{11},θ_{12}, and θ_{13}. A system of six equations in six variables is represented in Equation C.24. The variables are the Lagrange multipliers λ_i for $i = 1$ to 3; and the three actuator torques Q_j for $j = 4$ to 6.

It is noted that x, y, and z components of an external force exerted at the center of the moving platform are represented as the generalized forces, Q_i for $i = 1$ to 3. Therefore, three constraint equations are required. These equations arise from the fact that the length of the upper arm is always equal to the distance between joints B and C; that is

$$\begin{aligned} \Gamma_i = \overline{B_i C_i}^2 - b^2 &= (p_x + hcos\phi_i - rcos\phi_i - acos\phi_i cos\theta_{1i})^2 \\ &+ (p_y + hsin\phi_i - rsin\phi_i - asin\phi_i cos\theta_{1i})^2 \\ &+ (p_z - asin\theta_{1i})^2 - b^2 = 0 \quad for \quad i = 1 \; to \; 3 \end{aligned} \tag{C.27}$$

It is assumed that the mass of each connecting rod, m_b, in the upper arm assembly is divided evenly and concentrated at the two end points B_i and C_i in order to simplify the analysis. Then, the Lagrangian function, L, is derived as follows.

Total kinetic energy of the manipulator is

$$K = K_p + \sum_{i=1}^{3}(K_{ai} + K_{bi}) \tag{C.28}$$

where K_p is the kinetic energy of the moving platform, K_{ai} is the kinetic energy of the input link and the rotor on limb i, and K_{bi} is the kinetic energy of the two connecting rods of limb i. Specifically,

$$K_p = \frac{1}{2}m_p(\dot{p}_x^2 + \dot{p}_y^2 + \dot{p}_z^2)$$

$$K_{ai} = \frac{1}{2}(I_m + \frac{1}{3}m_a a^2)\dot{\theta}_{1i}^2$$

$$K_{bi} = \frac{1}{2}m_b(\dot{p}_x^2 + \dot{p}_y^2 + \dot{p}_z^2) + \frac{1}{2}m_b a^2 \dot{\theta}_{1i}^2$$

where m_p is the mass of the moving platform, m_a is the mass of the input link, m_b is the mass of one of the two connecting rods, and I_m is the axial moment of inertia of the rotor mounted on the i^th limb.

Total potential energy of the manipulator is

$$U = U_p + \sum_{i=1}^{3}(U_{ai} + U_{bi}) \tag{C.29}$$

where U_p is the potential energy of the moving platform, U_{ai} and U_{bi} are the potential energy of the input link and two connecting rods of limb i, respectively. Specifically,

$$U_p = m_p g_c p_z$$

$$U_{ai} = \frac{1}{2} m_a g_c a sin\theta_{1i}$$

$$U_{bi} = m_b g_c (p_z + a sin\theta_{1i})$$

Therefore, the Lagrangian function, L, is obtained

$$\begin{aligned} L = {} & \frac{1}{2}(m_p + 3m_b)(\dot{p}_x^2 + \dot{p}_y^2 + \dot{p}_z^2) + \frac{1}{2}(I_m + \frac{1}{3}m_a a^2 + m_b a^2)(\dot{\theta}_{11}^2 + \dot{\theta}_{12}^2 + \dot{\theta}_{13}^2) \\ & - (m_p + 3m_b) g_c p_z - (\frac{1}{2}m_a + m_b) g_c a (sin\theta_{11} + sin\theta_{12} + sin\theta_{13}) \end{aligned} \tag{C.30}$$

When the derivatives of Equation C.30 with respect to the six generalized coordinates are taken, it is obtained

$$\frac{d}{dt}(\frac{\partial L}{\partial \dot{p}_x}) = (m_p + 3m_b)\ddot{p}_x, \quad \frac{\partial L}{\partial p_x} = 0,$$

$$\frac{d}{dt}(\frac{\partial L}{\partial \dot{p}_y}) = (m_p + 3m_b)\ddot{p}_y, \quad \frac{\partial L}{\partial p_y} = 0,$$

$$\frac{d}{dt}(\frac{\partial L}{\partial \dot{p}_z}) = (m_p + 3m_b)\ddot{p}_z, \quad \frac{\partial L}{\partial p_z} = -(m_p + 3m_b) g_c,$$

$$\frac{d}{dt}(\frac{\partial L}{\partial \dot{\theta}_{11}}) = (I_m + \frac{1}{3}m_a a^2 + m_b a^2)\ddot{\theta}_{11}, \quad \frac{\partial L}{\partial \theta_{11}} = -(\frac{1}{2}m_a + m_b) g_c a cos\theta_{11}$$

$$\frac{d}{dt}(\frac{\partial L}{\partial \dot{\theta}_{12}}) = (I_m + \frac{1}{3}m_a a^2 + m_b a^2)\ddot{\theta}_{12}, \quad \frac{\partial L}{\partial \theta_{12}} = -(\frac{1}{2}m_a + m_b)g_c a cos\theta_{12}$$

$$\frac{d}{dt}(\frac{\partial L}{\partial \dot{\theta}_{13}}) = (I_m + \frac{1}{3}m_a a^2 + m_b a^2)\ddot{\theta}_{13}, \quad \frac{\partial L}{\partial \theta_{13}} = -(\frac{1}{2}m_a + m_b)g_c a cos\theta_{13}$$

When the partial derivatives of Equation C.27 with respect to the six generalized coordinates are taken, it yields

$$\frac{\partial \Gamma_i}{\partial p_x} = 2(p_x + hcos\phi_i - rcos\phi_i - acos\phi_i cos\theta_{1i}) \quad for\ i = 1, 2, and\ 3$$

$$\frac{\partial \Gamma_i}{\partial p_y} = 2(p_y + hsin\phi_i - rsin\phi_i - asin\phi_i cos\theta_{1i}) \quad for\ i = 1, 2, and\ 3$$

$$\frac{\partial \Gamma_i}{\partial p_z} = 2(p_z - asin\theta_{1i}) \quad for\ i = 1, 2, and\ 3$$

$$\frac{\partial \Gamma_1}{\partial \theta_{11}} = 2a[(p_x cos\phi_1 + p_y sin\phi_1 + h - r)sin\theta_{11} - p_z cos\theta_{11}]$$

$$\frac{\partial \Gamma_i}{\partial \theta_{11}} = 0 \quad for\ i = 2, and\ 3$$

$$\frac{\partial \Gamma_i}{\partial \theta_{12}} = 0 \quad for\ i = 1, and\ 3$$

$$\frac{\partial \Gamma_2}{\partial \theta_{12}} = 2a[(p_x cos\phi_2 + p_y sin\phi_2 + h - r)sin\theta_{12} - p_z cos\theta_{12}]$$

$$\frac{\partial \Gamma_i}{\partial \theta_{13}} = 0 \quad for\ i = 1, and\ 2$$

$$\frac{\partial \Gamma_3}{\partial \theta_{13}} = 2a[(p_x cos\phi_3 + p_y sin\phi_3 + h - r)sin\theta_{13} - p_z cos\theta_{13}]$$

When the derivatives above are substituted into Equation C.25 and C.26, a system of dynamical equations are obtained. For j=1, 2, and 3:

$$2\sum_{i=1}^{3} \lambda_i (p_x + hcos\phi_i - rcos\phi_i - acos\phi_i cos\theta_{1i}) = (m_p + 3m_b)\ddot{p}_x - f_{px} \tag{C.31}$$

$$2\sum_{i=1}^{3} \lambda_i (p_y + hsin\phi_i - rsin\phi_i - asin\phi_i cos\theta_{1i}) = (m_p + 3m_b)\ddot{p}_y - f_{py} \tag{C.32}$$

$$2\sum_{i=1}^{3} \lambda_i (p_z - asin\theta_{1i}) = (m_p + 3m_b)\ddot{p}_z + (m_p + 3m_b)g_c - f_{pz} \tag{C.33}$$

where f_{px} is the x component of an external force applied on the moving platform, f_{py} is the y component of an external force applied on the moving platform, and f_{pz} is the z component of an external force applied on the moving platform. For j=4, 5, and 6:

$$\begin{aligned} T_1 = (I_m + \frac{1}{3}m_a a^2 + m_b a^2)\ddot{\theta}_{11} + (\frac{1}{2}m_a + m_b)g_c a cos\theta_{11} \\ - 2a\lambda_1[(p_x cos\phi_1 + p_y sin\phi_1 + h - r)sin\theta_{11} - p_z cos\theta_{11}] \end{aligned} \tag{C.34}$$

$$\begin{aligned} T_2 = (I_m + \frac{1}{3}m_a a^2 + m_b a^2)\ddot{\theta}_{12} + (\frac{1}{2}m_a + m_b)g_c a cos\theta_{12} \\ - 2a\lambda_2[(p_x cos\phi_2 + p_y sin\phi_2 + h - r)sin\theta_{12} - p_z cos\theta_{12}] \end{aligned} \tag{C.35}$$

$$T_3 = (I_m + \frac{1}{3}m_a a^2 + m_b a^2)\ddot{\theta}_{13} + (\frac{1}{2}m_a + m_b)g_c a cos\theta_{13} \\ - 2a\lambda_3[(p_x cos\phi_3 + p_y sin\phi_3 + h - r)sin\theta_{13} - p_z cos\theta_{13}] \tag{C.36}$$

As it is mentioned before the Lagrange multipliers can be found from the first set of three linear equations, Equation C.31 through Equation C.33. Once they are found, the actuator torques can be determined from the second set of equations, Equation C.34 through Equation C.36.

APPENDIX D: AUTOMATION PRODUCTS

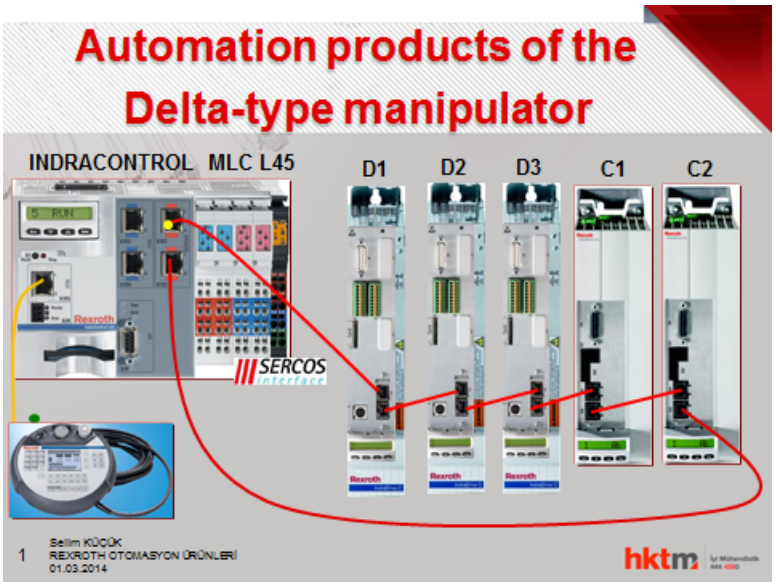

Figure D.1. Connection lines the automation products.

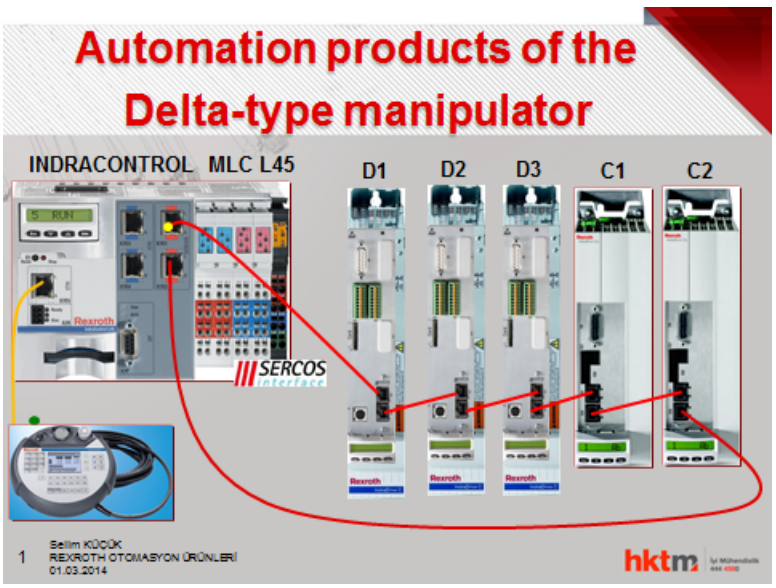

Figure D.2. Technical specifications of INDRACONTROL MLC L45.

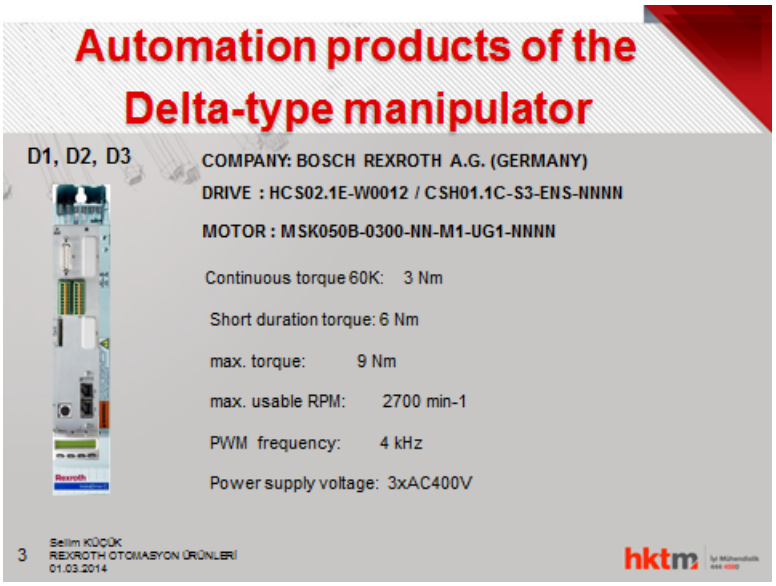

Figure D.3. Technical specifications of the actuators of the manipulator.

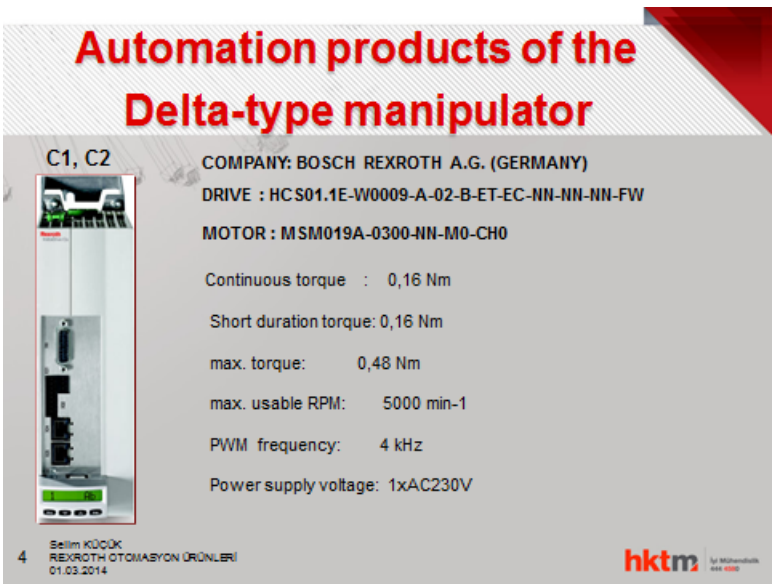

Figure D.4. Technical specifications of the motors of the 2-DOF gripper.

Figure D.5. Technical specifications of the manual operator panel.